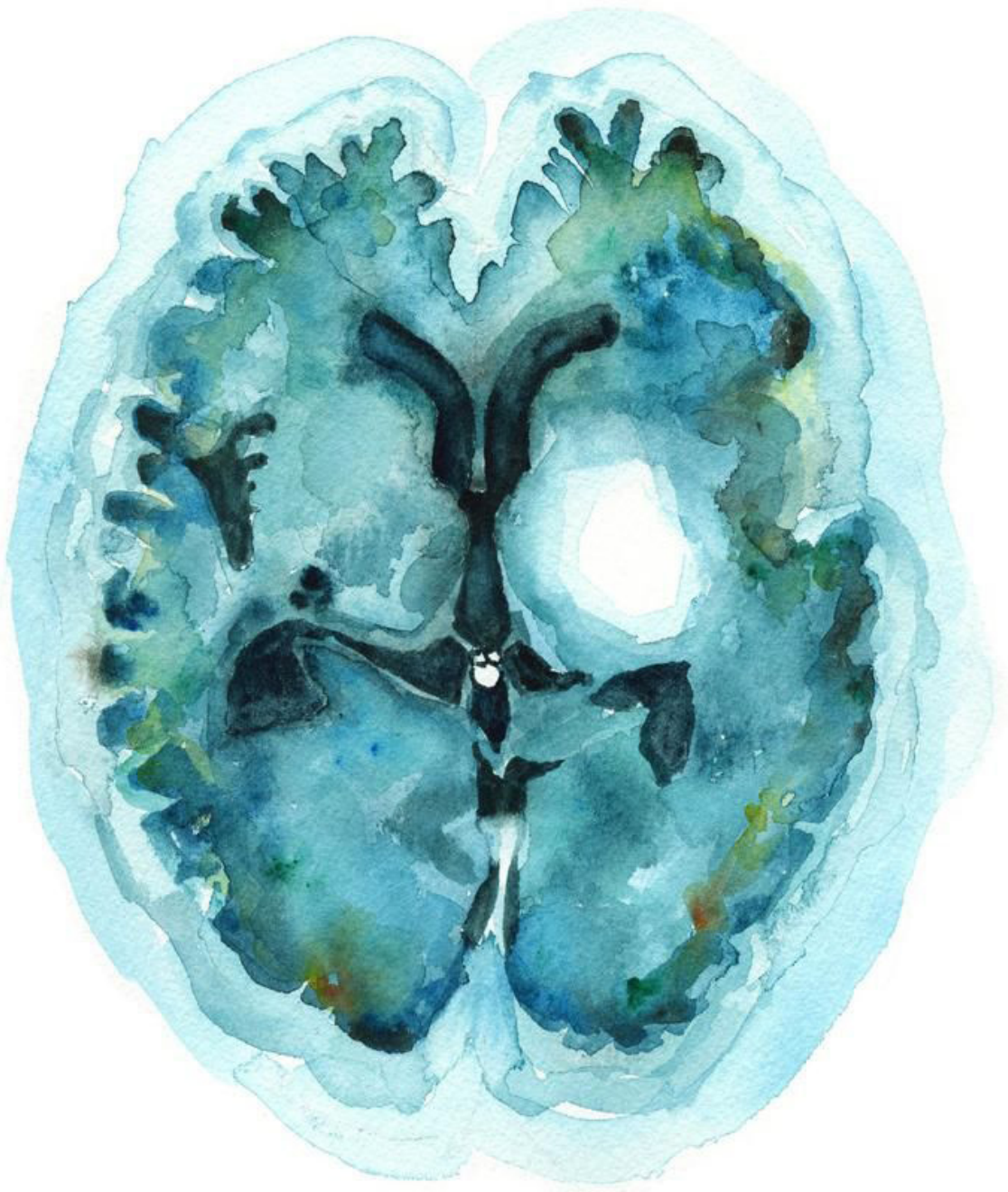# Development of a computational aspiration thrombectomy model:

## Application of a two-phase flow approach to describe thrombus behavior

E.L. van de Ven



**TU**Delft

Erasmus MC
University Medical Center Rotterdam

# Development of a computational aspiration thrombectomy model:

## Application of a two-phase flow approach to describe thrombus behavior

by

# E.L. van de Ven

to obtain the degree of Master of Science
at the Delft University of Technology,
to be defended publicly on Wednesday August 18, 2021 at 10:00 AM.

An electronic version of this thesis is available at `http://repository.tudelft.nl/`.

**TU**Delft

# Preface

This thesis is the result of the last academic year, where I was allowed to perform research at the Biomechanics Group of the Erasmus MC on a subject that I have always found interesting; the cardiovascular system. Performing research on a very new topic like thrombectomies can be very challenging, due to its recent breakthrough, but more importantly, it can be very interesting and rewarding, with a lot of room for improvement and future research. This thesis has challenged me in ways I hadn't experienced before and it is fair to say that it was accompanied by some ups and downs. Nevertheless, I am very grateful and proud to present my thesis.

This work would not have been the same without the support I received and therefore, I would like to thank a few people. First of all I would like to thank my supervisors, Frank Gijsen and Giulia Luraghi. Thank you for sharing your knowledge, answering all of my questions and for pushing me to dig deeper. I would also like to thank Rachel Cahalane for her additional guidance during this project. I am grateful for Suze-Anne Korteland and her help when LS-DYNA wasn't working as expected. To my master student colleagues at the Erasmus MC, Jo-Anne, Serena and Manouk, thank you for the fun times in the lab and for the teamwork and inspiration during the project. Furthermore, I would like to thank the members of my graduation committee for their time to evaluate my work.

Beside the academic and content related support, I have received a great amount of support from my nearest and dearest, which I value more than they know. Thank you to my parents, my sister, Ide, my roommates and my dear friends for always listening, cheering me up and celebrating the small and big victories with me.

*E.L. van de Ven*
*Delft, August 2021*

# Abstract

Acute Ischemic Stroke (AIS) is an abrupt onset of a focal neurological deficit due to the occlusion of a cerebral artery caused by thrombosis or embolism. According to the World Health Organization, stroke is the second leading cause of death in the world. One of the available treatments is the aspiration thrombectomy, where a negative pressure is applied to the thrombus in order to remove it from the vessel. In this work, the aspiration thrombectomy will be studied through the development of a computational model. By means of the development of this model, a baseline is created for exploratory research into both the technical and clinical aspects.

The range of applied thrombus models in literature varies largely. In this work, the thrombus is modelled using a fluid material model. Through the application of this fluid model, an emphasis is put on the fluid properties of thrombi, which exhibit both solid and fluid behavior. Three fluid models are applied, of which two represent non-Newtonian fluid behavior and one Newtonian fluid behavior. The effects of these material models are assessed through the pressure and velocity distribution and the thrombus behavior.

Furthermore, an evaluation of three clinical parameters, aspiration pressure, suction distance and thrombus length, is performed. Each parameter was assigned three variations, which are assessed based on the respective recanalization times. Each clinical parameter is evaluated to influence the recanalization time, albeit to different extents.

In conclusion, this thesis functions as exploratory research in the development of computational aspiration thrombectomy models. Future research is advised, in the form of material model verification with patient-retrieved or analog clots or more extensive research into the relation between recanalization time and the presented clinical parameters.

# Contents

# 1

# Introduction

## 1.1. Acute Ischemic Stroke

Acute Ischemic Stroke (AIS) is "an abrupt onset of a focal neurological deficit due to the occlusion of a cerebral artery" [1] as defined by the World Health Organization. Most of the acute ischemic strokes are thromboembolic [1], signifying a vessel blockage caused by a blood clot and shown in Figure 1.1. This blood clot, also referred to as thrombus, is the result of fibrin polymerization and the activation of platelets inside the circulatory system.[2] According to the World Health Organization, stroke is the second leading cause of death in the world.[1] Even if a patient survives a stroke, the consequences can be severe with patients suffering from hemiparesis, aphasia or generally not being able to take care of themselves anymore.[1] The importance of preventing and treating stroke can therefore not easily be underestimated. If an AIS occurs, the main goal is to remove the thrombus as fast as possible. A phrase often used in Neurology is "time is brain", highlighting the speed of tissue necrosis and its impact on nervous tissue.[3] This tissue necrosis speed furthermore has implications for the treatment itself, not only for timeframe from the onset of the AIS onwards in which treatment takes place for a patient. It is therefore of utmost importance to treat a patient suffering from AIS as quickly as possible.
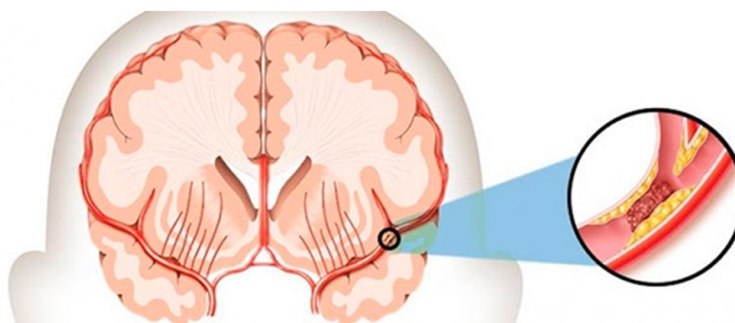


Figure 1.1: An illustration of Acute Ischemic Stroke (AIS), where a thrombus blocks a cerebral vessel

The initial treatment of AIS was intravascular thrombolysis [4] which is mostly alteplase.[5] As a result of the alteplase injection, the thrombus would be dissolved pharmacologically. However, this treatment alone has a low level of efficiency.[4] Mechanically removing the thrombus had a rise in popularity and efficacy for large vessel occlusions [6] after recent advancements, such as the Mr Clean trial in 2015.[7] In the current era, mechanical thrombectomy treatments of AIS can be divided into three groups; stent retriever thrombectomy, aspiration thrombectomy and a combination of both.[8] Mechanical thrombectomies have often been combined with thrombolysis to maximize the chances of a good outcome of the treatment.[5]

This thesis will focus on the aspiration thrombectomy. During this procedure, an aspiration catheter is brought to the occlusion site. A negative pressure is applied to the thrombus through the aspiration catheter, creating a suction force to remove the thrombus.[4] A schematic representation of this procedure is shown in Figure 1.2 This negative pressure is usually applied by means of a syringe or a vacuum pump.[9] The aspiration procedure itself has several variations in the actual procedure, e.g. the thrombus can be fully ingested in the catheter or only partially during retraction, the catheter can have direct contact with the thrombus or no contact.



Figure 1.2: An illustration of the aspiration thrombectomy. The aspiration catheter (left) inside the vessel is approaching the thrombus (dark red), which is stuck in the vessel shown on the right.

Various approaches exist to study AIS and aspiration thrombectomy. In vivo studies can be conducted, where the stroke and treatment are analyzed inside the patient's body. However, because of the critical impact of time between the stroke onset and treatment, it is a difficult task to perform studies in this time window. An alternative research approach is to perform in vitro studies, where AIS and the treatments of AIS are studied outside a patient's body. Because of technological advancements, a third option to perform studies has become available, namely in-silico studies. In-silico studies make use of numerical models to study the mechanisms of AIS and potential treatments.[10] Numerical models of stroke treatments always develop later than their clinical counterpart [11], creating a delay between the clinical application and the respective in-silico studies. However, in-silico models have a broad potential for different applications and studies (e.g. combining an in-silico model with a population of virtual patients allowing for in-silico trials, adapting the treatment to the patient-specific parameters and needs or the improvement of devices [12]). By conducting numerical research on AIS treatment, the goal is to acquire a deep understanding of the thrombectomy procedure to eventually improve the treatment and the design of thrombectomy devices in a later phase. A numerical model will be used in this thesis to study the aspiration thrombectomy.

## 1.2. Related work

Current in-silico studies concerning aspiration thrombectomy are scarce, with nine found papers conducting numerical studies of aspiration procedures. In these studies, the influence of various parameters is investigated. The outcomes used to assess the influence of these parameters are mainly recanalization and resul-

tant suction force on the thrombus. Recanalization is defined as the reopening of an occluded vessel [13] and can be assessed on the basis of recanalization time (i.e. time until the vessel is completely reopened) or recanalization percentage (i.e. the percentage of the vessel that is reopened). The investigated parameters in literature are mainly aspiration pressure, suction distance, catheter model and thrombus material model. These parameters can be divided into two categories, where one category is related to the clinical practice (i.e. aspiration pressure, suction distance, catheter model) and one category related to the representation of the clinical practice in the computational model (i.e. thrombus model).

### 1.2.1. Clinical Practice

The used aspiration pressure in current literature ranges from 10 kPa to 100 kPa. In all studies with varying aspiration pressures, higher aspiration pressure values resulted in higher or better recanalization.[14]–[17] An example of this is shown in Figure 1.3. According to Soleimani *et al.* [16], the maximum tolerable pressure value for vessels is 100 kPa, based on the study of Romero *et al.* [18]. This maximum value is established on the idea that aspiration pressure values can potentially damage the vessel wall [18] and therefore the aspiration pressure can't be increased infinitely. The applied aspiration pressures in this thesis will be 30 kPa. This relatively low value was opted for, in order to be able to observe the thrombus behavior during aspiration as much as possible, without employing the smallest aspiration value.
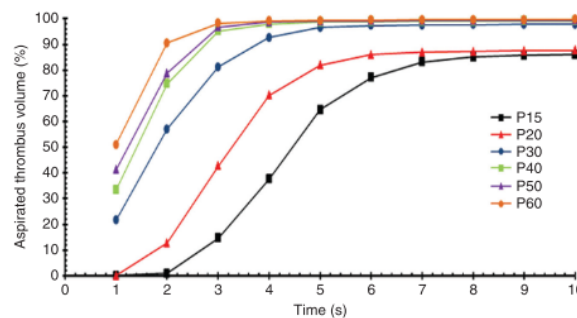


Figure 1.3: In the study of Soleimani et al. [16] higher aspiration pressures generate quicker aspiration and higher recanalization ratios. The aspiration pressure range from 15 kPa to 60 kPa and are indicated by the different curves. For each aspiration pressure, the recanalization time (x-axis) and recanalization percentage (y-axis) are shown.

The applied suction distances range from 0.0mm to 5.0mm in literature. Generally, the tendency leans towards "the closer, the better" with regards to suction distance and the resultant suction force.[14], [17], [19] A topic of disagreement between various authors, is whether or not direct contact between the thrombus and catheter is favourable. Generally, most of the studies did not have direct contact between the thrombus and the catheter. Nevertheless, the influence of suction distance on the recanalization has not been investigated extensively and is therefore a potentially interesting topic of research.

In literature, few different catheter models are studied, with the Penumbra catheters being the most predominant. Based on the information of the MR CLEAN Registry [20], the Penumbra catheters are furthermore the most used catheters in the medical practice, together with the Sofia catheters.

### 1.2.2. Thrombus Model

The range of applied thrombus models varies largely in literature. Examples are a solid barrier [19], a deformable porous tissue [15], a hyperelastic material [21], a viscoelastic material [22] or a second, very viscous fluid [16], [23], [24]. Furthermore, the characterization of material properties of retreived thrombi from patients has shown a large variation of properties and composition between thrombi [25] as can be seen in Figure 1.4.
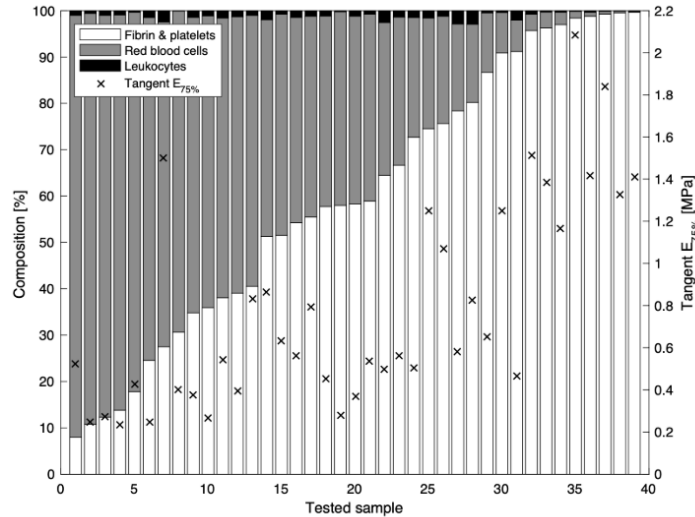


Figure 1.4: The composition of 40 retreived thrombus samples from patients in the thesis of Philip Snouckaert van Schauburg[25]. It shows a large variation in the composition of thrombi, together with a broad variation of E moduli.

Representing the range of mechanical properties of thrombi is a necessary step for future in-silico trials with a virtual population. For now, creating a material model that mimics the behavior of one specific thrombus, including characteristics like fragmentation and anisotropy, is the first step that needs to be taken in the process of developing a computational aspiration thrombectomy model. In this thesis, an alternative approach to the various solid material models in literature will be used by applying a fluid material model to the thrombus. This approach, also known as the two-phase flow approach [26], models both the blood and the thrombus as fluids and was preceded by the work of Soleimani *et al.* [16], Pennati *et al.* [23], and Neidlin *et al.* [24]. The main ground for this decision is based on the nature of an aspiration thrombectomy, which lies in the removal of a thrombus from its occlusion location, inherently requiring large deformations. Solid material models typically make use of Lagrangian element formulations, where large deformations of the solid material are accompanied by large element distortions.[27] On the contrary, fluid materials usually apply an Eulerian element formulation, allowing large deformations of the material without distortions.[27] Consequently, a fluid material model was considered to meet the large deformation requirements of an aspirated thrombus better than its solid opponents. Using a fluid material approach furthermore bypasses the requirement of a fluid-structure interaction coupling mechanism between a solid thrombus and the blood in order to include a solid thrombus in the model. The fluid material model thus also results in a computationally less expensive model. An additional advantage of this approach is the inclusion of thrombus fragmentation. Fragmentation of the thrombus can result in distal embolization [28], which is one of the large difficulties encountered during a thrombectomy and therefore a very relevant feature to include. The combination of these arguments led to the choice of the two-phase flow approach to describe thrombus behavior.

## 1.3. Research Aim

Due to the scarcity of in-silico studies concerning aspiration thrombectomies, the main goal of this thesis is to create a numerical aspiration thrombectomy model merging the information of current literature. A two-phase flow approach has not yet been combined with a Penumbra catheter, a defined suction distance and an aspiration pressure range between 10 and 100 kPa. Furthermore, no baseline model is currently available and therefore this development is necessary in order to investigate specific parameters. Secondly, the fluid thrombus material model will be explored further. As discussed earlier, no representative thrombus material model has yet been developed and therefore, in order for computational models to deliver meaningful insights about the medical procedure, it is important to continue the exploration and development of these numerical models. Similar to solid material models, fluid behavior can be expressed through various material models. In this thesis, three viscosity models will be compared, examining the difference in thrombus behavior in order to advance the search for a fitting thrombus material model for future research. Lastly, the previous research will lead to the examination of the effect of three clinical parameters on the thrombus behavior in the developed computational model. These three parameters are: aspiration pressure, suction distance and thrombus length. Their results will be assessed on the recanalization time. These three parameters could provide meaningful information for the medical practice, since it relates outcome of the procedure to information that is present during the medical intervention and which is either patient-specific (thrombus length) or variable during the procedure (aspiration pressure, suction distance). The study of these parameters allow preliminary recommendations to be made towards the medical practice of aspiration thrombectomies.
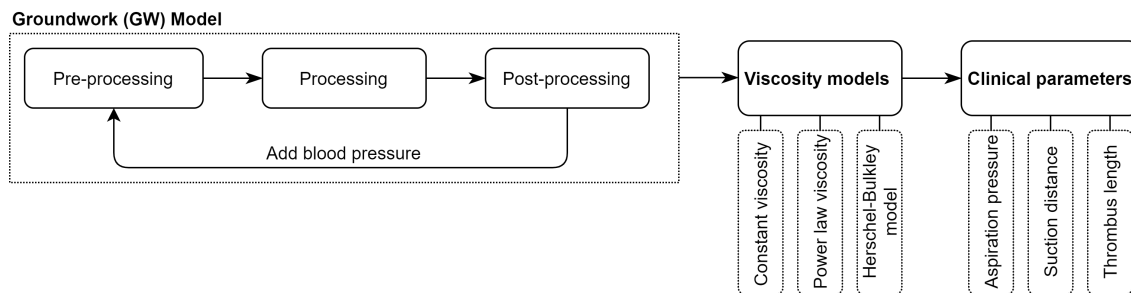
## 1.4. Thesis Outline



Figure 1.5: The illustrated workflow of this thesis, showing the three separate segments. First, a groundwork model is developed, after which three viscosity models are implemented and compared. Lastly, three clinical parameters are varied and their effect on the recanalization time is assessed.

The first part of this thesis consists of the development of the numerical analysis of the aspiration thrombectomy. The workflow of this numerical analysis is shown in Figure 1.5. First of all, the pre-processing part takes place, in which the geometry, the discretization of the geometry, the material model and boundary conditions are defined. Due to the complexity of this numerical analysis, a groundwork (GW) model is developed, consisting of the fluid thrombus material, a rigid catheter and vessel walls and an applied aspiration pressure of 30 kPa. The pre-processing is executed with LS-PrePost [29]. Secondly, this GW model simulations are run, using the explicit finite element solver LS-DYNA (ANSYS)[29]. This software is opted for, because of its Arbitrary Langrangian-Eulerian formulation options fitting well with the goal of this thesis to model the thrombus as a second viscous fluid. Subsequently, the results are assessed during the post-processing phase. This is done using LS-PrePost [29] and ParaView [30]. Once this GW model is pre-processed, processed and post-processed, the model is further optimized by adding a blood pressure. This approach of adding blood

pressure secondly is opted for in order to increase the complexity of the analysis gradually. Afterwards, three different viscosity models are assessed and compared as thrombus material models. Lastly, three different clinical parameters (aspiration pressure, aspiration distance, thrombus length) are varied in order to investigate their influence on the recanalization time. Chapter 2 describes the numerical analysis of the GW model, with the addition of blood pressure, Chapter 3 describes the three viscosity models and their results and ultimately, Chapter 4 reports the comparison of the three clinical parameters.

# 2

# Numerical Analysis

## 2.1. Geometry

The created geometry is a simplified representation of an aspiration thrombectomy procedure with a vessel, a thrombus and an aspiration catheter. The vessel was modelled as a straight cylindrical tube, which is a simplification of reality considering that the M1 segment of the Middle Cerebral Artery (MCA) is not straight. The M1 segment of the MCA was chosen as the occlusion location, since this is where most of the thrombus occlusions take place [20] and is shown in Figure 2.1. The exact dimensions of the M1 segment of the MCA are patient-specific and therefore variable. A value of 3.0 mm was chosen as the vessel diameter based on previous computational studies.[14], [15], [31]
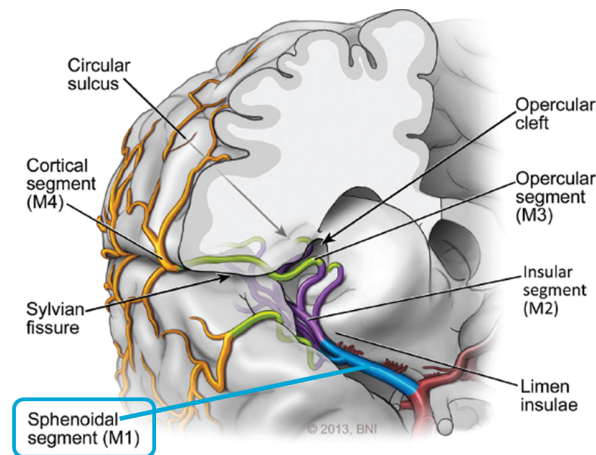


Figure 2.1: The M1 segment (blue) of the Middle Cerebral Artery (MCA), where most of the thrombus occlusions are located [20]

The created geometry for the GW model, is shown in Figure 2.2. The geometry consisted of the following parts: thrombus, aspiration catheter, vessel wall, blood and a part to apply aspiration pressure. Because of a smaller computational load and assumed symmetry, only half of the vessel and thrombus were modelled. The catheter geometry was based on the Penumbra 5MAX catheter [32], since Penumbra catheters are most frequently used, based on the information of the MR CLEAN Registry [20]. This is

10 errors7 warnings also in accordance with the study of Chitsaz *et al.* [15]. The vessel diameter is 3.0 mm with a vessel length of 10 mm. The thrombus is 100% occlusive and therefore also has a diameter of 3.0 mm, with a length of 5.0 mm. The average thrombus length in the clinical setting amounts 18.0 mm. To reduce the computational load, a thrombus length of 5.0 mm was chosen. In future research, it could be interesting to use a larger thrombus length because of this difference with the average value. [33]. Additionally, the influence of different thrombus lengths will be investigated in Chapter 4.
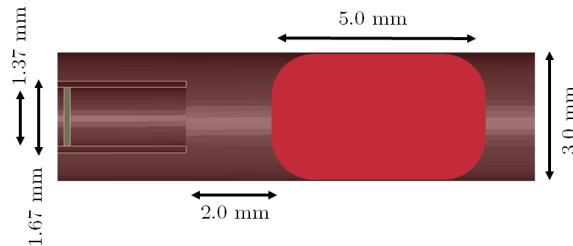


Figure 2.2: The modelled geometry of the aspiration thrombectomy, with the thrombus (red), the aspiration catheter on the left, the vessel wall and the part to apply the aspiration pressure (green)

## 2.2. Mesh

In order to discretize the geometry, a mesh was generated for the geometry described in Section 2.1. Various types of meshes can be applied, dividing the original geometry in different types of finite elements. In this analysis, a hexahedral mesh was used in the fluid and the rigid parts (catheter and vessel wall), which is the suggested mesh type for ALE formulations.[34] The mesh type of the thrombus container was triangular. The meshed geometry is shown in Figure 2.3
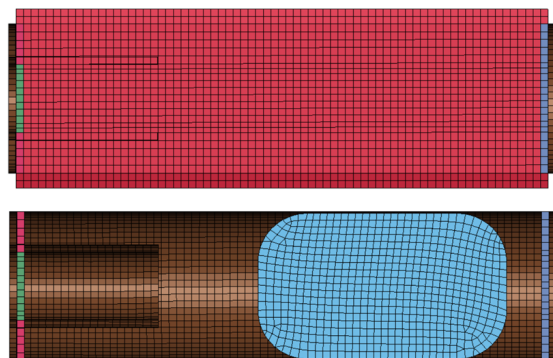


Figure 2.3: The meshed geometry for the blood domain (upper image) the rigid parts and the thrombus (lower image). The hexahedral mesh for the blood and rigid parts is shown, together with the triangular mesh for the thrombus container (light blue).

## 2.3. Fluid Thrombus

In order to model the thrombus as a fluid, the blood and thrombus need to be distinguished as two different, yet interfering fluid domains. This was done using specific LS-DYNA commands that allow the fluid domain to be initialized with two different fluid materials (blood and the thrombus).

### 2.3.1. ALE Multi-material Group

First of all, two fluid groups (blood & the thrombus) are defined. These fluid groups represent the different material entities that can flow throughout the simulation and are defined using the *ALE multi-material group* command of LS-DYNA.[35] Since the thrombus is located inside the blood, the initial location of the thrombus needs to be defined and this is done using a shell part (i.e. the thrombus "container") with the dimensions of the thrombus described in Section 2.1. Marking the initial thrombus location is the only task of this thrombus "container" and other than that, this part will have no influence on the simulation. The relationship between the two fluids, alongside the location of the thrombus within the blood, is defined using the *Initial Volume Fraction Geometry* command of LS-DYNA.



Figure 2.4: A representation of the two fluid groups and the thrombus container, which assigns the initial location of the thrombus material inside the vessel.

### 2.3.2. Element Formulation

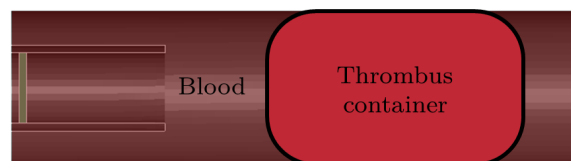The used element formulation in this model was Eulerian for the blood and the thrombus, which is specific instance of the Arbitrary Lagrangian-Eulerian formulation, where the velocity of the reference mesh is equal to 0.[27] The Eulerian element formulation allows the material to "flow" through the mesh elements and thus, elements can contain different materials at different points in time. This is in contrary to the Lagrangian element formulation where the mesh moves and deforms together with the material.

The structural parts (i.e. the catheter, vessel wall and thrombus container) were modelled as shells and make use of a Lagrangian formulation, more specifically a Belytschko-Tsay element formulation, implying that these parts are not able to flow through the mesh. As will be discussed in Subsection 2.3.3, the materials for these parts were modelled to be rigid and therefore have no displacement.

### 2.3.3. Materials

Three materials were used in this model; a rigid material and two fluid materials. The rigid material will be used for the thrombus container, the vessel wall and catheter and this material is constrained in the x,y and z direction for both displacement and rotation.

Initially, a Newtonian fluid material was applied for both the thrombus and the blood. This Newtonian fluid material was applied to the blood throughout the complete thesis. The thrombus material will be altered later in this thesis, which is discussed in Chapter 3. The assigned density and viscosity for both the thrombus and blood are displayed in Table 2.1. Both the blood and the thrombus were modelled to be incompressible fluids, using a linear polynomial equation of state.

Table 2.1: Viscosity ($\mu$) and density ($\rho$) values for blood and the thrombus.These parameters are based on the study of Neidlin *et al.* [24]

| Blood viscosity $\mu_b$ | Blood density $\rho_b$ | Thrombus viscosity $\mu_t$ | Thrombus density $\rho_t$ |
|---|---|---|---|
| 0.0036 kg/m.s | 1056.4 kg/m$^3$ | 0.036 kg/m.s | 1300 kg/m$^3$ |

### 2.3.4. Fluid-Structure Interaction

Since both solid and fluid parts were present in the model, a coupling mechanism was required to define the fluid-structure interaction. This mechanism defines the coupling between the blood on the one hand and the catheter and vessel wall on the other hand. The used LS-DYNA command (*Constrained Lagrange in solid*) was specifically aimed to allow couplings between Lagrangian and Eulerian parts, where a fluid master and a solid slave are defined. The master was in this case the catheter with the vessel wall and the slave was defined as the blood. A penalty coupling mechanism was applied for this interaction.

This fluid-structure interaction allowed the thrombus to be modelled 100% occlusive. If no fluid-structure interaction was present, indicating that no solid part would represent the catheter or the vessel wall, the nodes of the blood at the vicinity of the vessel wall would have to be fixated in order to constrain the blood and the thrombus in a physical space that represents the vessel. A similar operation would be required to represent the catheter. However, if the thrombus would be modelled to be 100% occlusive in that case, the outer nodes of the thrombus would be fixated together with the fixated nodes of the blood, since these are coinciding. This implies that the thrombus material near the vicinity of the vessel wall could never be aspirated because of this fixation. If no solid parts would be introduced in this model, the thrombus would have to be scaled down not to be occlusive anymore, leaving a small layer of blood between the thrombus and the vessel wall. This would allow the thrombus to move freely towards the catheter during aspiration. However, when evaluating this against the reality of an AIS, the model would resemble the medical practice less, since non occlusive thrombi are less likely to get "stuck" and cause an acute ischemic stroke. Therefore, the choice was made to introduce solid parts, requiring a penalty coupling mechanism and increasing the computational load and complexity.

### 2.3.5. Boundary Conditions

Two types of boundary conditions were defined in this computational model. The first one is a specific node set contraint. With the model assumed to be symmetric in the zy plane, it was possible to only model a half of the vessel, thrombus and catheter to reduce the computational time. Because of this half geometry, it was required to constrain the xy plane. Therefore, the constraint was applied to a node set, consisting of all nodes in the symmetry plane located coincident with the x- and y-axis. The node set coincident with the y-axis was constrained translationally in z direction and rotationally about the x- and y-axis.

The second boundary condition was the application of the negative aspiration pressure on the blood. The applied aspiration pressure for the GW model follows a linear curve until the respective aspiration pressure is reached, starting at 0 kPa and reaching the respective aspiration pressure at t=250 ms. The aspiration pressure curve for an aspiration pressure of -30 kPa is shown in Figure 2.5. The aspiration pressure is applied to the *Aspiration Part* shown in Figure 2.2 in green and is located inside the catheter, on the left end of the catheter.
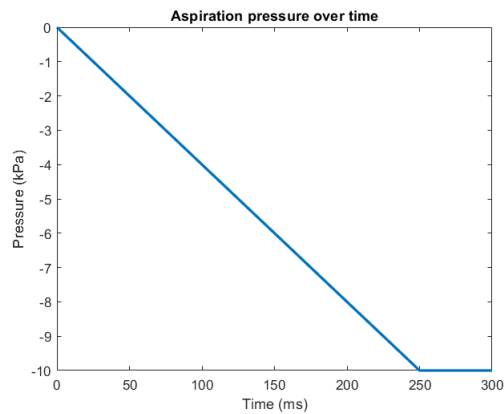
Figure 2.5: The aspiration pressure curve for the GW model starting at 0 kPa and reaching -30 kPa at t=250ms.

### 2.3.6. Mesh Sensitivity Analysis

To explore the influence of mesh element size on the results, a mesh sensitivity analysis was conducted. This analysis was done by comparing the results of three identical models with different mesh element sizes. In this case, the selected element sizes were 0.05 mm (Mesh A), 0.10 mm (Mesh B) and 0.15 mm (Mesh C) for all domains. The meshes were created for identical geometries with identical boundary conditions, including a blood pressure of 12 kPa and an aspiration pressure of -30 kPa.
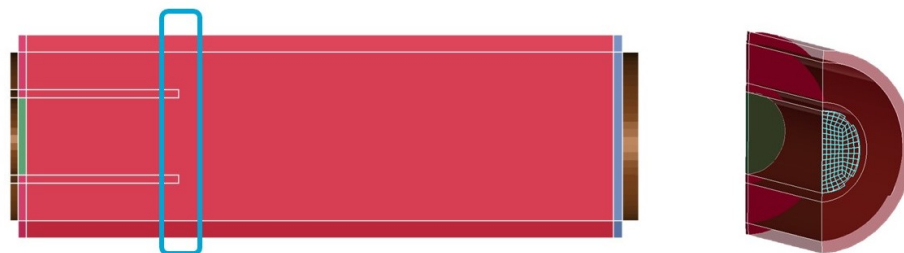


Figure 2.6: The element selection used for the quantitave mesh sensitivity analysis, located inside the catheter tip. In the left image, the location of the section is shown. In the right image, the element selection in this section is shown.

The compared parameters for the different element sizes are pressure and resultant velocity. The results were assessed in a qualitative and quantitative manner. In order to analyze the results of the mesh sensitivity analysis in a qualitative way, the velocity and pressure profiles at t=250 ms were compared. For the quantitative analysis, the average value for a selection of elements was compared. This selection of elements is shown in Figure 2.6 and is located at the catheter tip, inside the catheter. Both the average resultant velocity ($\overline{v}$)and the average pressure ($\overline{P}$) were calculated for this element selection. Because this is a transient analysis, with boundary conditions changing over time, the average pressure and resultant velocity values were compared at two points in time; t = 50 ms and 250 ms. For both parameters, the error percentage was calculated with Equation 2.1 for the difference between the 0.15mm mesh and the 0.10mm mesh on the one hand, and the 0.10 mm mesh and the 0.05 mm mesh on the other hand.

The aim of the mesh sensitivity was to have a mesh size that is small enough for the results to not change extensively when the element size of the mesh is decreased. This difference between the different mesh sizes

can be observed through the error percentage.

$$ErrorPercentage = \frac{\overline{P}(Larger\,mesh) - \overline{P}(Smaller\,mesh)}{\overline{P}(smaller\,mesh)} \cdot 100 \qquad (2.1)$$

## 2.4. Processing & Post-Processing

The models were run using LS-DYNA R.12. [29] In order to reduce the computational time, Message Passing Parallel (MPP) was used with 4 CPUs. The used computer was a *Dell Precision 5820 Desktop* with 32 GB RAM provided by Erasmus MC. The post-processing was executed with LS-PrePost [29] and Paraview [30].

## 2.5. Blood Pressure

As mentioned earlier in this chapter, the complexity of the analysis was increased gradually. In the initial GW model, no blood pressure was present which was implemented as a blood pressure equal to 0 kPa. However, in reality blood and its inherent blood pressure are part of the thrombectomy procedure. Since the thrombus is extracted by the application of a negative pressure, a complete understanding and application of the pressure present in this procedure is important and includes the blood pressure together with the aspiration pressure. A pressure of 12 kPa was applied to the complete blood domain, based on Shi *et al.* [19] and was applied through the linear polynomial equation of state. Due to the increased blood pressure, the aspiration pressure curve for the new model starts at 12 kPa at t = 0 ms instead of 0 kPa after which it linearly decreases to the respective aspiration pressure at t=250 ms. This can be seen in Figure 2.7 , showing the new aspiration pressure application curve. This GW model with a blood pressure of 12 kPa will be referred to as the GWB model.
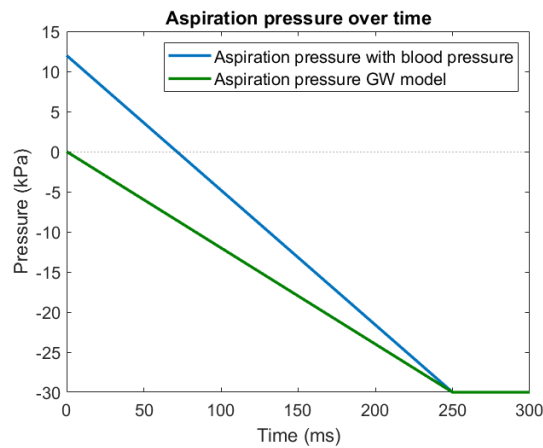


Figure 2.7: An illustrative aspiration pressure curve for the GW model starting at 0 kPa and reaching -30 kPa at t=250ms. An illustrative aspiration pressure curve for the GWB model is shown in blue, starting at 12 kPa and reaching -30 kPa at t=250ms.

## 2.6. Results

In the following section, the results for GW Model including the thrombus are shown, together with the results of the GWB model with the thrombus and the mesh sensitivity analysis.

### 2.6.1. Groundwork Model (GW)



Figure 2.8: The thrombus kinematics (left), pressure distribution (middle) and velocity distribution including the velocity vectors (right) over time of the GW model with an aspiration pressure of 30 kPa.

Figure 2.8 shows the pressure and velocity distribution, together with the thrombus kinematics for the GW model with an aspiration pressure of 30 kPa. The thrombus kinematics display the thrombus in red and the blood domain in blue. Here, it is observed that the thrombus moves towards the catheter, after which it is gradually aspirated. The distal end of the thrombus maintains its shape until 80 ms, after which the thrombus segments near the vessel wall remain in their place while the central part is aspirated. At 110 ms, the thrombus is completely removed from the vessel.

In the pressure distribution, the gradual pressure decrease caused by the aspiration pressure on the left side of the catheter can be observed. Over time, it can be seen that the decreasing pressure values, caused by the applied aspiration pressure, propagate through the fluid starting at the application location of the pressure and ending in the region around the catheter tip. No negative pressure is located outside the catheter tip. The thrombus is removed from the vessel after 110 ms, when the aspiration pressure has not reached its final value of 30kPa yet, indicating that the thrombus is aspirated with an aspiration pressure smaller than 30 kPa. The maximum aspiration pressure before full aspiration of the thrombus (i.e. at t=100 ms) is 12.1 kPa, following the applied boundary condition.

This gradual decrease in aspiration pressure results in increasing velocities inside the catheter, causing the thrombus to be aspirated. Increasing velocity values are observed over time, with a maximum value of 9.0 m/s
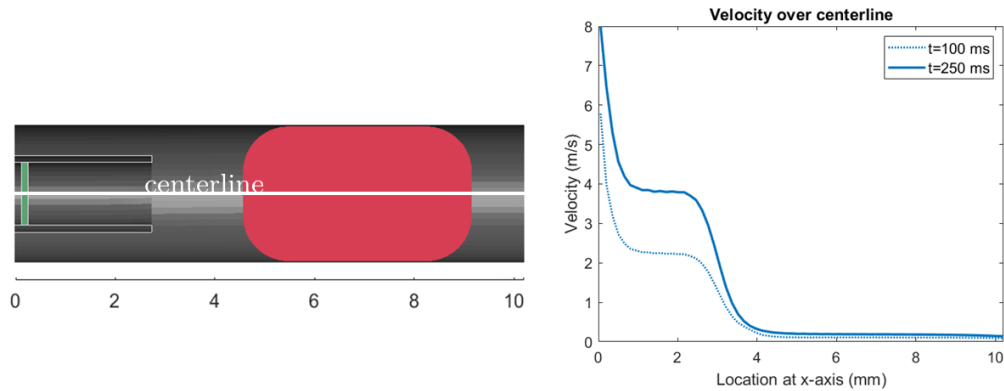
Figure 2.9: The velocity values over the centerline at t=100 ms and t=250 ms. The location of the centerline, accompanied by the measurements at the bottom in mm, is shown on the left. The resultant velocity values over this centerline are displayed in the graph on the right. The x-axis presents the location over the centerline in mm and the y-axis displays the resultant velocity value in m/s.

at t=250 ms inside the catheter at the aspiration application location. The velocity over the centerline is shown in Figure 2.9 for the velocities at t=250 ms and right before the thrombus is completely aspirated, at t=100 ms. Both curves initially start at their respective maximum values, quickly decreasing to a plateau for the location between 1.4 mm and 2.1 mm on the x-axis. This plateau corresponds to $2.2 m/s$ for t=100ms and $3.8 m/s$ for t=250 ms. Nearing the tip of the catheter, between 2.1 and 4.0 mm on the x-axis, the velocity steeply decreases a second time, after which the resultant velocity remains stagnant at a value of approximately $0.1 m/s$ for t=100 ms and $0.2 m/s$ for t=250ms. This signifies that the high velocity values of this curve are mainly located inside the catheter and that the velocity values very quickly decrease outside of the catheter to a fraction of the velocities inside the catheter. The increased velocities extend to a location of approximately 1.0 mm outside of the catheter. Additionally, it can be observed in the velocity profile that a change of direction occurs near the catheter tip for blood in the proximal area of the vessel. This likely signifies the aspiration of blood from both the distal and proximal area of the vessel.

## 2.6.2. GW Model With Blood Pressure (GWB)
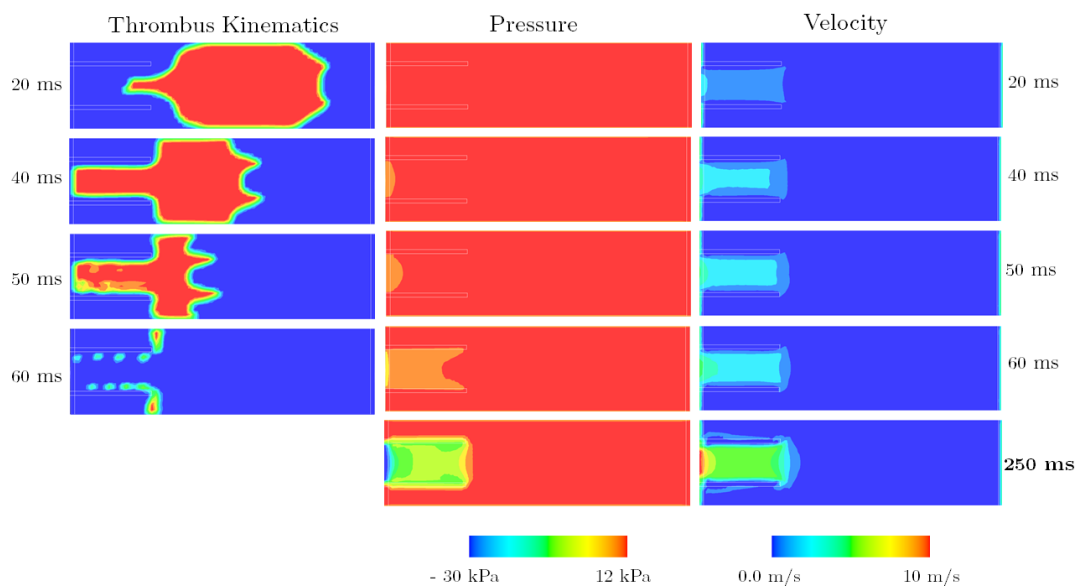
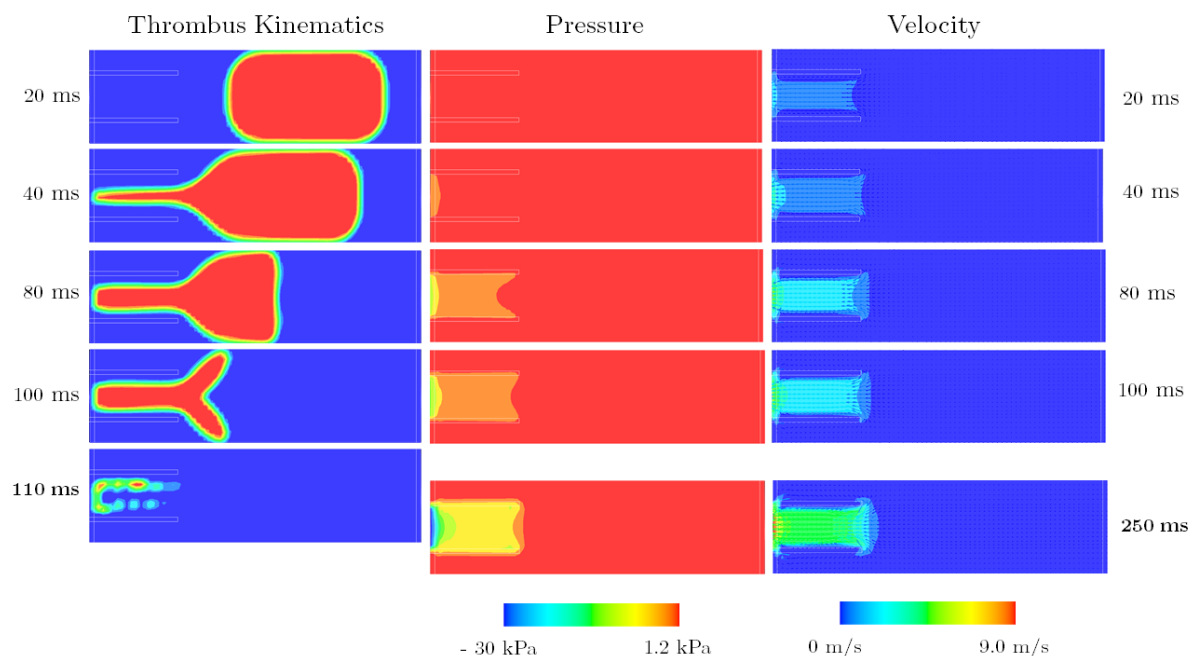

Figure 2.10: The thrombus kinematics (left), pressure distribution (middle) and velocity distribution (right) over time of the GWB model with a blood pressure of 12 kPa and an aspiration pressure of 30 kPa.

The results of the GWB model with a thrombus and added blood pressure are shown in Figure 2.10. In the thrombus kinematics, it can be observed that the thrombus is aspirated due to the aspiration pressure in this model as well. The thrombus moves towards the catheter, after which it is gradually aspirated. At t=60 ms only fragments located at the catheter tip remain inside the vessel, obstructing the connection between the proximal and distal part of the vessel. Additionally, the shape of the thrombus during aspiration differs from the thrombus shape in the previous model, despite the fact that the material properties of the thrombus are identical. When the thrombus is already partly inside the catheter, the catheter creates an angle of approximately 90° in the transition between the thrombus segment inside the catheter and the one outside of the catheter. This transition caused an angle larger than 90° in the GW model without blood pressure. Furthermore, at the distal end of the thrombus, an indentation is visible located in the center of the thrombus end. This indentation is already present at t=20 ms and deepens over time.

In the pressure distribution, it can be observed that a gradual pressure decrease propagates through the catheter. When the thrombus is largely aspirated at 60 ms, a substantial pressure decrease has just reached the catheter tip. At this time, the applied aspiration value has reached 1.9 kPa, implying that the thrombus is aspirated with a positive aspiration pressure value. However, a pressure gradient is still present, due to the difference of 1.9 kPA with the applied blood pressure of 12 kPa.

The velocities gradually increase over time, with the most visible velocity increases located inside the catheter. Decreasing pressure values inside the catheter over time are accompanied by larger velocities, and eventually at t=250 ms the highest velocities are located inside the catheter, with lower velocities extending to a location of approximately 1.0 mm outside of the catheter. Increased velocities are observed at the proximal part of the blood domain, next to the catheter. This likely signifies the aspiration of blood in the proximal domain of the vessel. In Figure 2.11, the velocity over the centerline is shown for the GWB model at t=50 ms, right before

Figure 2.11: The velocity values over the centerline at t=50 ms (i.e. the last moment before recanalization) and t=250 ms for the GWB model. The graph also displays the velocities over the centerline for the GW model w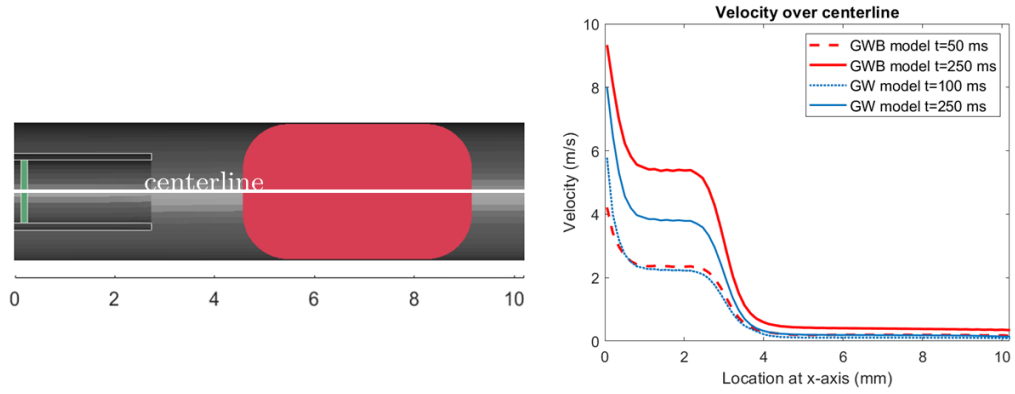ithout blood pressure at t=100 ms and t=250 ms. The location of the centerline, accompanied by the measurements at the bottom in mm, is shown on the left. The x-axis of the graph presents the location over the centerline in mm and the y-axis displays the resultant velocity value in m/s.

recanalization, and at t=250 ms. In this velocity curve, two steep velocity decreases can be seen, toghether with two plateaus located inside and outside the catheter, similar to the velocity over the centerline for the GW model. The locations of the plateaus and steep decreases are at identical for both the GW model and the GWB model, signifying a large velocity decline outside of the catheter. The velocity values of the GWB model at t=250 ms are higher, with an initial velocity of 9.0 $m/s$, a plateau inside the catheter of 5.3$m/s$ and a new plateau of approximately 0.4 $m/s$ outside the catheter. However, the velocity curves right before recanalization (i.e. at t=100 ms for the GW model and at t=50 ms for the GWB model) are very similar.

### 2.6.3. Mesh Sensitivity

The computational time of the three models with different element sizes, using Message Passing Parallel (MPP) with 4 CPUs and 32 GB RAM, is shown in Table 2.2. A non-linear increase of computational time is observed for the decreased element size.

Table 2.2: Computational time for the three different meshes. For each mesh, MPP was used with 4 processors and 32 GB RAM.

| Mesh | Mesh size | Computational time |
| --- | --- | --- |
| C | 0.15 mm | 3 hours 15 minutes 17 seconds |
| B | 0.10 mm | 10 hours 33 minutes 50 seconds |
| A | 0.05 mm | 95 hours 27 minutes 32 seconds |

The results of the qualitative analysis can be seen in Figure 2.13 and 2.12. In these figures, the pressure gradient is visible, ranging from the aspiration pressure of -30 on the left side of the catheter, to 12 kPa in the blood domain outside the catheter. The transition from -30 kPa to increased pressure values is largely located inside the catheter, with increasing pressure values for more distal locations of the aspiration application location. The blood domain outside of the catheter shows a constant pressure value of 12 kPa.

Figure 2.12: The pressure distributions of the 0.05 mm, 0.10 mm and 0.15 mm meshes compared at t=250 ms.The upper halves of the velocity profiles are placed side by side, with the one half mirrored in order to evaluate the velocity profile more easily.
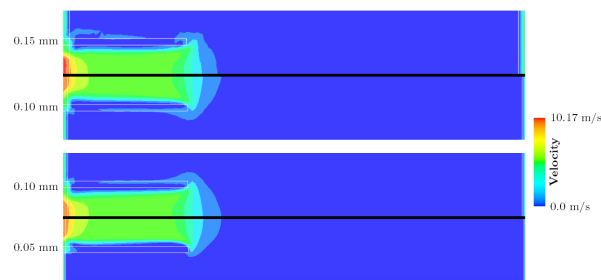


Figure 2.13: The velocity profiles of the 0.05 mm, 0.10 mm and 0.15 mm meshes compared at t=250 ms.The upper halves of the velocity profiles are placed side by side, with the one half mirrored in order to evaluate the velocity profile more easily.

In the qualitative analysis, it is observed that the velocity outside the catheter is very low in all meshes and starts increasing near the tip of the catheter. The velocity field is relatively similar for all three of the meshes, with the highest velocity where the pressure is applied, near the left side of the catheter and a decrease of velocity towards the catheter tip. An increased velocity is present outside of the catheter, located approximately 1.0 mm from the catheter tip. Furthermore, the maximum resultant velocity at the left end of the catheter is higher in the 0.15 mm mesh ($10.17 m/s$) than it is in the 0.05 mm mesh ($9.0 m/s$).

The pressure distribution in the qualitative analysis is relatively similar for all three of the meshes and all within the range of -30 kPa to 12 kPa, which corresponds to the applied pressure values (i.e. the negative aspiration pressure of 30 kPa and a blood pressure of 12 kPa). The lowest negative pressure values are located at the left end of the catheter, where the negative pressure is applied through the boundary conditions. This area furthermore corresponds to the location of the highest velocities in the velocity profile of figure 2.13.
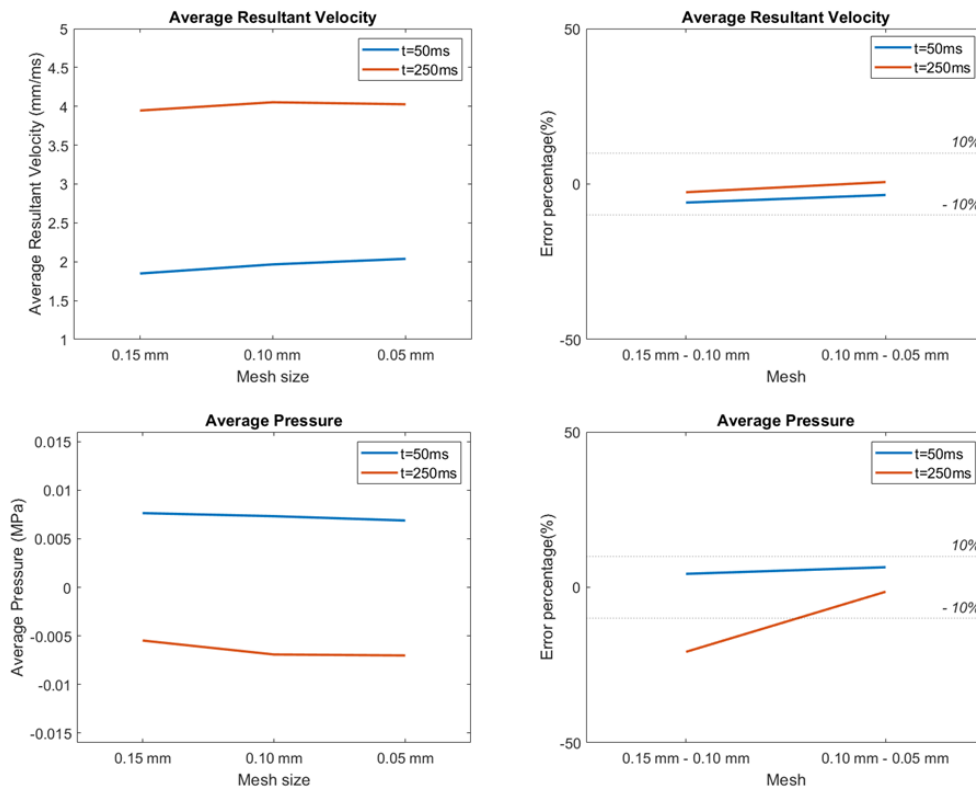
Figure 2.14: The quantitative analysis of the mesh sensitivity study. For both the resultant velocity (upper images) and the average pressure (lower images), the absolute values are shown on the left for t=50 ms and t=250 ms for all three mesh sizes. The right images show the error percentages for the resultant velocity and pressure at t=50 and t=250 ms, calculated with Equation 2.1.

Different graphs displaying the pressure and resultant velocity values at t=50 ms and t=250ms for the three mesh sizes, with a decreasing element size are shown in Figure 2.14. Furthermore, the error percentage between the different meshes is shown for the pressure and velocity values at t=50 ms and t=250ms. The shown values represent the average value in the element selection (i.e. the selected blood domain inside the catheter tip) , shown in Figure 2.6. The average resultant velocity graph shows error percentages smaller than 10% for both t=50 ms and t=250 ms. The average pressure error percentage is 1.42% between the 0.10 mm and the 0.05 mm mesh at t=50 ms and 20.77% between the 0.15 mm and the 0.10 mm mesh at t=250. This relatively large error percentage value at t=250 ms is likely influenced by the area location of the element selection. The selection is located at the catheter tip, which is the transition area between the negative aspiration pressure and the positive blood pressure inside the vessel, which comprises a large pressure gradient. Next to this transition, this area is subject to directional changes of the blood entering the catheter. This makes the location a complex region, susceptible to potential deviations.

Based on the results of both the qualitative and the quantitative analysis of the mesh sensitivity study, it can be concluded that small differences occur between the different mesh sizes. However, due to the large computational load that accompanies the mesh sizes of 0.10 and 0.05mm, the choice was made to apply a 0.015 mm mesh for the models in this thesis. This choice was furthermore supported by the fact that this thesis is exploratory research and therefore mainly focuses on the overall conclusions, contrary to hypotheses based on exact pressure or velocity values. The difference of the exact values between the different meshes is thus tolerated. Not to mention, the qualitative analyses demonstrate very similar pressure and velocity profiles, substantiating the 0.15mm mesh as the selected mesh size for the aim of this thesis.

## 2.7. Discussion

Both the GW model and the GWB model achieve a full aspiration of the thrombus, caused by the applied aspiration pressure. A gradual pressure decrease is displayed inside the catheter, initiated by the aspiration pressure and resulting in increased velocities inside the catheter. This is the case for both models. Although both thrombi are completely aspirated, the velocities measured outside of the catheter are substantially lower than those inside the catheter for both models. Regardless of these lower velocity values outside of the catheter, the thrombus is aspirated in both models, at aspiration pressures of -12.1 and 1.9 kPa.

With a recanalization time of 60 ms for the GWB model, the thrombus is aspirated 45% quicker than in the GW model. Furthermore, a higher resultant velocity of $10 m/s$ compared to the $9.0 m/s$ in the model with 0 kPa blood pressure is computed. Not only is the maximum resultant velocity higher for the GWB model, the velocity values located throughout the catheter are generally higher than those inside the catheter of the GW model. This could be explained by the larger pressure gradient that is present in the GWB model, with a 12 kPa blood pressure on the one hand and -30 kPa aspiration pressure on the other hand. A larger pressure gradient results in greater flow, according to the relationship between pressure gradients and flow.[36] This can furthermore be related to velocities, since flow ($q$) is proportionate to velocity ($\overline{v}$).[36] A larger flow thus causes larger velocities, as observed in the results. Furthermore, increased velocity values are present in an additional area in the GWB model, namely between the catheter and the vessel wall. This is also likely caused by the increased pressure gradient.

In the comparison of the velocity over the centerline, both velocity curves follow a similar trajectory, with two steep decreases enclosing a velocity plateau inside the catheter. This trajectory shape is present in both models at all points in time, yet with different velocity values. It is noteworthy that both velocity curves are almost identical right before full recanalization, although this is at very different points in time (i.e. at t=100 ms for the GW model and t=50 for the GWB model).

The pressure gradient of negative values, causing the thrombus to be aspirated, is largely located inside the catheter. No large pressure decreases can be observed in the blood domain outside the catheter. The increase of velocity during aspiration is also mainly located inside the catheter and near the vicinity of the catheter tip. This is also demonstrated by the velocity over the centerline, where a steep decrease of velocity occurs at the end of the catheter. Based on the results of this model, the velocities caused by the aspiration pressure inside the vessel (i.e. 0.2 $m/s$ and 0.4 $m/s$ over the centerline) are considered to be very small, since the velocity range extends to 10 $m/s$ inside the catheter. It could therefore be considered remarkable that the thrombus is aspirated as quickly as it is. However, if the velocity values inside the vessel are compared to what is considered the "normal" velocity range inside the MCA of 0.35 $m/s$ to 0.9 $m/s$ [37]–[39], 0.2 and 0.4 $m/s$ don't appear to be extremely small values anymore. Compared to this normal velocity range, the velocities inside the catheter are considered to be very high. The velocity range might be extended by the very high extremes inside the catheter of 10 $m/s$, making it look as if only negligible velocities are present inside the vessel. This is thus not the case, with the generated velocities inside the vessel being in the same order of magnitude of the normal velocity range of the MCA[37]–[39].

The different thrombus shapes for the GW and GWB model can be described by the difference in viscosity, which can be defined as "a fluid's resistance to flow" [40]. The thrombi in this model and the previous one

can thus be considered to be equally resistant to flow, since an identical viscosity is applied. Greater flows are present in this model due to the increased pressure gradient, causing larger deformations of the thrombus to take place in the GWB model.

The range of recanalization time until maximum recanalization is achieved in the study of Soleimani *et al.* [16] is between 2 and 5 seconds for aspiration pressures between 15 and 60 kPa. If this is compared to the recanalization time of 60 ms in the GWB model with 30 kPa aspiration, it is apparent that there is a discrepancy between the recanalization time of the created model in this thesis and the results of Soleimani *et al.* [16]. The recanalization time for 30 kPa specifically in the study of Soleimani *et al.* [16] is 4 seconds, which is more than 60 times the recanalization time of the created model in this thesis of 60 ms. Although the comparison is not completely equal, with a suction distance that was not specified and different aspiration catheters and thrombi models that were used in the study of Soleimani *et al.* [16], the difference in the order of magnitude of the recanalization time gives a hint that recanalization time could potentially be higher. One of the main factors influencing the recanalization time is considered to be the thrombus-vessel wall interface. It is now modelled using a penalty coupling mechanism.However, this is a simplification of the interface between the two tissues and it is suggested that the interface between the vessel wall and the thrombus could be modelled more fittingly. In order to do so, it is strongly encouraged to investigate the thrombus-vessel wall relationship more deeply.

### 2.7.1. Limitations & Simplifications

Various simplifications were applied to this model. First of all, the vessel was assumed to be a perfect cylinder and rigid. In reality, vessel dimensions and shapes vary between patients, together with the fact that cerebral vessels are rarely perfectly straight. This can be seen in Figure 2.15, where an CTA scan of a patient is shown.[41] Moreover, modelling the vessel to be rigid is a simplification of vessel wall tissue. Reducing the vessel wall to a rigid surface therefore neglects the specific vessel wall properties that play a role during the aspiration and moreover, it neglects the interaction between the thrombus and the vessel wall.
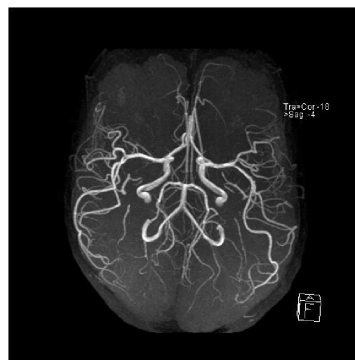


Figure 2.15: A CTA scan of a patient, showing the cerebral vessels and their geometry. [41]

A second simplification is the assumption of blood being a Newtonian fluid. Generally, it could be stated that blood is a non-Newtonian fluid with shear thinning behavior.[42] As mentioned previously, the aim of this model was to gradually build up complexity. Furthermore, with the main focus on the thrombus and its behavior in this thesis, it was opted to pick the thrombus as the subject of different fluid models. Simplifying the blood by using a Newtonian model was the choice that was made based on this research aim. The as-

sumption of the thrombus being a Newtonian fluid is a simplification that will be discussed in Chapter 3.

The last simplification concerns the blood pressure. In the current model, the blood pressure is assumed to be equal throughout the blood domain. However, in an AIS, the blood pressure is likely to differ between the domain distal and proximal to the thrombus. Due to the blockage of the vessel by the thrombus, the proximal blood pressure is likely to increase in contrary to the area distal of the thrombus, where no new blood can be transported towards because of the occlusion. Therefore, it would be assumed to be logical if the blood pressure proximal of the thrombus is higher, since blood is transported to this location yet obstructed by the thrombus, than the blood pressure distal to the thrombus, where no new blood is transported to.

### 2.7.2. Future Work

Various options arise for future work, by enhancing or improving the current model or by expanding the model with additional components. The first potential improvement of the model is based on the element size of the mesh. In this thesis, the main argument for the applied element size of 0.15 mm was the available computational load. If a larger computational load could be applied in the future for this model, it could be relevant and advised to utilize a smaller mesh size. As can be seen in the mesh sensitivity analysis, the velocity and pressure profile for the different mesh sizes are relatively similar. However, the absolute pressure and velocity values vary for the smaller mesh sizes. If more specific research questions concerning the exact values of pressure, velocity or another parameter, are to be investigated in the future with this model, it would be encouraged to apply a smaller mesh size.

Secondly, it could be interesting to adapt the made simplifications in order to resemble reality closer. This was already mostly discussed in Subsection 2.7.1, yet enhancements such as patient-specific geometry of the vessel or thrombus, non-Newtonian behavior to model blood or including vessel wall mechanics could be interesting improvements of the model that take it one step closer to reality.

Lastly, additional components could be added to the model such as a stent-retriever or a balloon guide catheter (BGC). Both components are devices used during thrombectomies, in combination with the aspiration catheter.[5] In future research, it could be interesting to compare the different thrombectomy approaches (e.g. stent-retriever or aspiration only, a combined approach, adding the BGC) and investigate their added value without having to use patients for the study itself. Eventually, the goal of in-silico studies is to improve the treatment and investigate the added value of different enhancements of the procedure itself. Nevertheless, the current goal is still to create a model that mimics reality as close as possible.

# 3

# Thrombus viscosity models

Biological materials often exhibit both elastic behavior, associated with solid materials and viscous behavior, associated with liquid materials.[43], [44] This is also the case for thrombi.[25] Due to the heterogeneous composition of thrombi [33] and moreover the deviation of properties between patient-specific thrombi [25],the characterization of thrombi is a complex task. In this thesis, the fluid behavior of thrombi was emphasized with a focus on viscosity, modelling the thrombus as a fluid. In order to do so, three different viscosity models were applied.

## 3.1. Power Law Model

First of all, a power law model, representing non-Newtonian fluid behavior, was selected as thrombus material model. Non-Newtonian fluids are defined by a viscosity that is shear strain rate dependent. An example of non-Newtonian fluid behavior is shear thinning, which signifies a decrease in viscosity for an increasing shear strain rate.[44] Shear thinning behavior can be described by a power law viscosity model, where the viscosity ($\mu$) is a function of shear strain rate ($\dot{\gamma}$) to the power $n-1$, multiplied by a constant ($K$).

$$\mu = K\dot{\gamma}^{n-1} \tag{3.1}$$
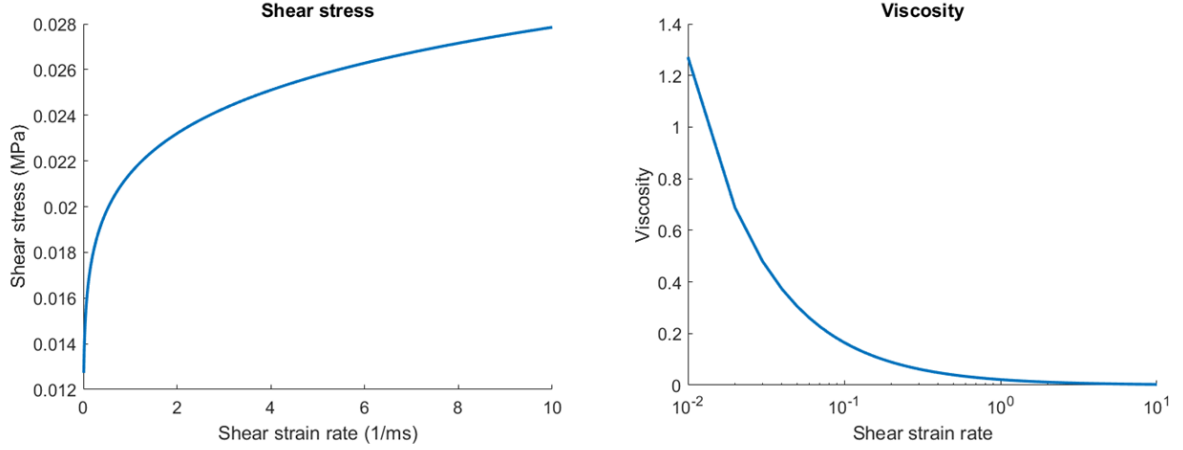
Figure 3.1: The shear stress-shear strain rate relation of the power law model (left) and the viscosity-shear strain rate relation (right) are shown.

To apply this model to the thrombus, $K$ and $n-1$ were chosen based on the article of Soleimani *et al.* [16], who apply a power law viscosity to model thrombus behavior. In this article, three types of thrombi are distinguished: a thrombus with a low viscosity (LV), a thrombus with a medium viscosity (MV) and a thrombus with a high viscosity (HV), all modelled using a power law viscosity model. Since the comparison of thrombus material models in this thesis aimed to focus on the fundamental differences between the different material modes and how a thrombus can be modelled the best, one type of thrombus was chosen to use from the study of Soleimani *et al.* [16], namely the low viscous thrombus (LV). The according values are shown in Table 3.1, together with the representing viscosity and shear stress curves of a shear thinning fluid in Figure 3.1.

Table 3.1: $K$ and $n$ values based on Soleimani *et al.* [16]

| Thrombus | $K$ | $n$ |
|---|---|---|
| Low viscosity (LV) | 0.02145 | 0.1134 |

## 3.2. Herschel-Bulkley Model

The second viscosity model also represents non-Newtonian fluid behavior. The Herschel-Bulkley model demonstrates solid-like behavior at low shear strain rates and once the yield stress is passed, the material will start to flow, showing fluid-like behavior.[44] This yield stress is the stress threshold that distinguishes the solid-like phase from the fluid-like phase, where shear stresses induce shear rates once this threshold is passed.

The Herschel-Bulkley model is expressed through Equation 3.2, where the viscosity ($\mu$) is equal to the constant $\tau_0$, divided by the shear strain rate ($\dot{\gamma}$), added by the constant factor ($k$) multiplied by the shear strain rate ($\dot{\gamma}$), divided by the critical shear strain rate ($\dot{\gamma}_c$), to the power ($n-1$).

$$\mu = \frac{\tau_0}{\dot{\gamma}} + k(\frac{\dot{\gamma}}{\dot{\gamma}_c})^{n-1} \tag{3.2}$$
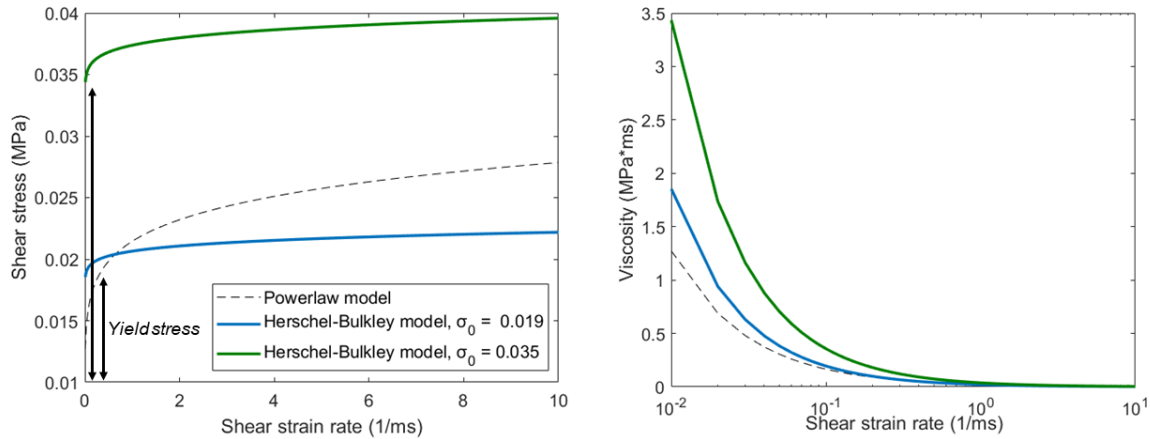
Figure 3.2: The shear stress-shear strain rate relation for the two sets of material parameters for the Herschel-Bulkley thrombus model (left) and the viscosity-shear strain rate relation (right) are shown, compared to a power-law model with identical $K$ and $n$ values. The intersection between the power law model curve and the blue Herschel-Bulkley curve can be observed at a shear strain rate of $0.65 ms^{-1}$.

The shear stress-shear strain rate curve of a Herschel-Bulkley model is shown in Figure 3.2. Here, it can be observed that, contrary to the power law model, shear strain rates only occur once the yield stress is passed. Below this yield stress, the material will behave as if it were solid, with very little strain. In order to estimate the correct parameters required for the Herschel-Bulkley model, the shear stress-shear strain rate curve was compared to the curve of the power law function. Since the Herschel-Bulkley model also makes use of a power law function to model the fluid, the multiplication constant ($k$) and exponent ($n-1$) values are identical to the values used in the power law model in Section 3.1. No previous work was found to support defining $\tau_0$ and the critical shear strain rate ($\dot{\gamma}_c$) for thrombi using the Herschel-Bulkley model. The shear strain rates ($\dot{\gamma}$) in the thrombus with a low viscous (LV) power law viscosity were observed. During aspiration, the maximum average shear strain rate inside the thrombus was approximately $0.65 ms^{-1}$. Therefore, the choice was made to let both the shear stress-shear strain rate curves intersect at a shear strain rate of $0.65 ms^{-1}$ in order to represent relatively similar thrombi. This can be seen in Figure 3.2. Consequently, $\tau_0$ was set at 0.0155 and the critical shear strain rate ($\dot{\gamma}_c$) was set at $0.2 ms^{-1}$. This results in a yield stress ($\sigma_0$) of $0.019 MPa$ that distinguishes the solid-like behavior from the fluid-like behavior and the thrombus with this parameter set will be referred to as the low yield stress (LYS) thrombus. After assessing the results, a second set of parameters was determined in order to compare the difference with the originally defined material parameters. The aim of this second set of parameters was to get a broader overview of how a thrombus with a Herschel-Bulkley material model would behave and what the impact was of the defined parameters. In order to do this, the second set of parameters was chosen to differ largely from the first set of values, with a determined yield stress of $0.035 MPa$, which is almost double the yield stress of the original values. The thrombus with these parameters will be referred to as the high yield stress (HYS) thrombus. The accompanying material parameters $\tau_0$ and $\dot{\gamma}_c$ are shown in Table 3.2.

Table 3.2: The defined $K$, $n$, $\tau_0$ and $\dot{\gamma}_c$ values for the Herschel-Bulkley model. $K$ and $n$ are based on Soleimani *et al.* [16], $\tau_0$ and $\dot{\gamma}_c$ are pragmatically defined. Two different yield stresses are modelled with these parameters.

| Thrombus | Yield Stress ($\sigma_0$) | $K$ | $n$ | $\tau_0$ | $\dot{\gamma}_c$ |
|---|---|---|---|---|---|
| LYS | 0.019 MPa | 0.02145 | 0.1134 | 0.0155 | 0.2 |
| HYS | 0.035 MPa | 0.02145 | 0.1134 | 0.03 | 0.3 |

## 3.3. Constant Viscosity Model

Lastly, a Newtonian fluid model was applied to model the thrombus in order to compare the non-Newtonian fluid behavior of the thrombus to a relatively simple baseline of a Newtonian fluid model. Newtonian fluids linearly relate the shear stress ($\sigma$) of a fluid to the shear strain rate ($\dot{\gamma}$).[44] This constant viscosity model was also applied in the GW and GWB model.

$$\sigma = \mu\dot{\gamma} \qquad (3.3)$$

A constant viscosity value of $0.036\frac{kg}{m.s}$, which is 10 times more viscous than blood ( $0.0036\frac{kg}{m.s}$ [24]) and a density of $1300kg/m^3$ were chosen based on Pennati $et\ al.$ [23]. When comparing the behavior and viscosity value of these values to the behavior and the different viscosities for different strain rates in the power law model described in Section 3.1, it is apparent that the constant viscosity value is much lower ($0.036\frac{kg}{m.s}$) than any of the values in the power law model. Therefore, a new constant viscosity was defined. Initially, an attempt was made to deduct a viscosity from the power law curve (e.g. a viscosity of $21.5\frac{kg}{m.s}$ at a shear strain rate of $1.0ms^{-1}$). However, viscosity values in this order of magnitude resulted in out-of-range forces in LS-DYNA, with an error termination of the model as a result. Consequently, the original viscosity value of $0.036\frac{kg}{m.s}$ was multiplied by 60 in order to obtain a viscosity that differed substantially and in two orders of magnitude with the original value, without resulting in an error termination. The newly acquired viscosity value was $2.15\frac{kg}{m.s}$. This value furthermore corresponded to the viscosity value of the power law model at a shear rate of $13ms^{-1}$.

## 3.4. Results

In the following section, the results of the three different viscosity models will be shown and discussed.

### 3.4.1. Power Law Viscosity



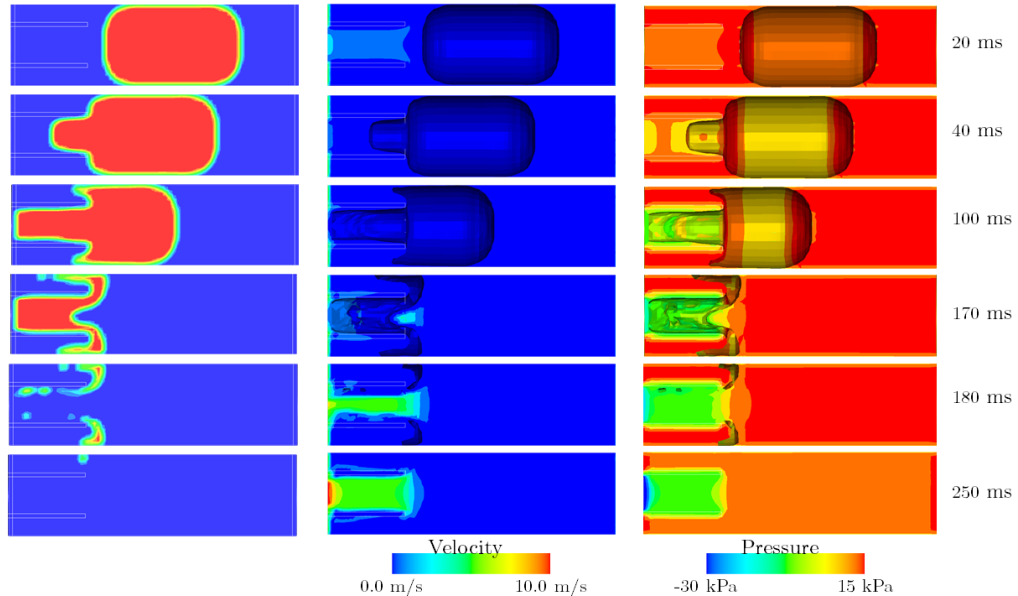Figure 3.3: The aspiration of the power law model thrombus (left), the velocity profile during aspiration (middle) and the pressure distribution during aspiration (right) with an aspiration pressure of -30 kPa. In the velocity and pressure profile, the contour of the thrombus is shown during aspiration. The colours mapped inside this thrombus contour signify the velocity and pressure values in the blood domain behind the thrombus.

In Figure 3.3, the thrombus kinematics of the power law thrombus material model can be observed over time, together with the pressure and velocity profile. The thrombus is initially pulled towards the catheter, after which it is gradually aspirated, until no thrombus parts remain in the vessel. It takes 20 ms for the thrombus to be retracted to the catheter tip and 180 ms in total for the thrombus to be completely aspirated. Once the thrombus is partly inside the catheter, thrombus parts near the vicinity of the vessel wall move into the area between the catheter and the vessel wall and are the last parts to remain inside the vessel before complete aspiration. During aspiration, the section of the thrombus located in this part of the vessel increases until the thrombus is aspirated and removed from the vessel.

In the velocity profile, it is observed that an increased velocity is present in the catheter during aspiration, before any segment of the thrombus enters the catheter. Once a segment of the thrombus has entered the catheter, only very small velocities are located inside the catheter. After the aspiration of a large part of the thrombus, with only fragments remaining outside of the catheter at t=180 ms, increased velocity values are observed inside the catheter. At t=250 ms, the velocity profile has become identical to the one of the GW model with blood pressure.

In the pressure distribution shown in Figure 3.3, the applied aspiration pressure gradually reaches its final value of -30 kPa, following the applied aspiration pressure curve. The highest absolute value for the aspiration pressure that is reached when the thrombus is not yet aspirated is -16.5 kPa, at the left side of the catheter. The blood domain outside of the catheter has a pressure range between 6 kPa and 15 kPa. This maximum value of 15 kPa is higher than the assigned blood pressure value of 12 kPa and could be caused by the separation of the distal and proximal side of the blood domain. This separation of the distal and proximal part is caused by remaining thrombus fragments inside the vessel and results in increased pressure values for the proximal part of the blood. Additionally, it is observed that the layer of blood directly on the distal side of the thrombus has a lower pressure value once the thrombus is almost aspiration at t=170ms. After full recanalization, the pressure inside the catheter continues to increase and eventually a pressure distribution is reached where the blood outside of the catheter has a pressure value of 10 kPa.

## 3.4.2. Herschel-Bulkley Model

In Figure 3.4 a comparison is shown of the thrombus kinematics for the LYS and HYS thrombi. With recanalization times of 180 and 190 ms for the LYS and HYS thrombi respectively, the aspiration time only differs very slightly between the two models. During aspiration, the behavior of the thrombi is almost identical, with the exception of the time frame of 20 ms before full aspiration, where the HYS thrombus preserves its original shape at the distal side a little more than the LYS thrombus. In Figure 3.4 the first principle stresses are also shown for the thrombi. Although the thrombus shapes are relatively similar during aspiration, it is noticeable that the HYS thrombus has extensively larger stresses inside the thrombus. The stresses for both thrombi are shown with a minimum and maximum range of -11 kPa and 110 kPa respectively. The minimum and maximum first principle stress values for the LYS thrombus are -5 kPa and 75 kPa. The stress distributions of the two thrombi have similar trends, albeit with separate stress values. During aspiration it can be observed that a slightly rectangular area occurs in the stress distribution, where positive and negative stresses alternate. This rectangular shape extends from the proximal side of the thrombus to the distal side of the thrombus, in an extension of the catheter. For both thrombi, the highest stresses occur when more than half of the thrombus is already aspirated or in the catheter and this maximum stress is located inside the catheter, near the tip or
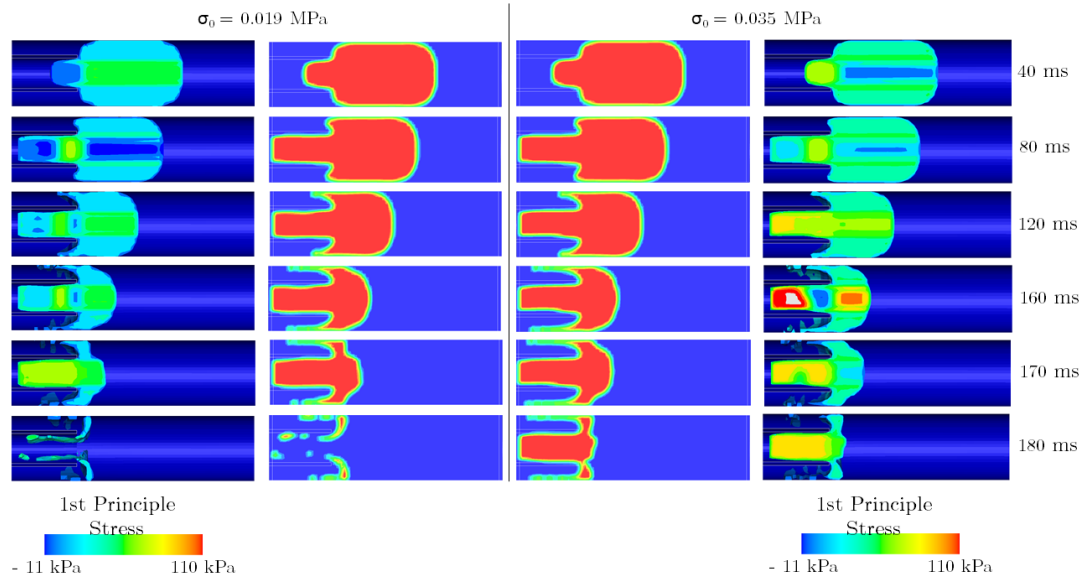
Figure 3.4: A comparison of the two material parameter sets applied for the Herschel-Bulkley model. Both the thrombus kinematics and the first principle stress are shown. The parameter set that results in a yield stress of 0.019 MPa is shown on the left and the parameter set resulting in a yield stress of 0.035 MPa is shown on the right.

located 0.5mm inside the catheter.

In Figure 3.5, the velocity and pressure profile of the HYS thrombus are shown. Similar to the velocity profile of the power law model, an increased velocity inside the catheter is observed, until the thrombus is partly inside the catheter. During aspiration, low velocities are observed inside the catheter. Once the thrombus is largely aspirated, higher velocities occur, with a maximum of $10\,m/s$ located at the left side of the catheter. The pressure distribution shows the increase of the pressure inside the catheter during the aspiration, following the applied aspiration curve (i.e. shown in Figure 2.7). When the thrombus is partly located in the vessel during aspiration, a small pressure increase in the proximal blood domain between the catheter and the vessel wall is present. The elevated pressure in this area ranges from 12 kPa (i.e. the initially assigned blood pressure) to 15 kPa. Due to the chosen minimum and maximum values, this increased pressure is not fully visible in Figure 3.5. However, when the largest volume of the thrombus is aspirated at 190 ms, it becomes visible that a pressure difference is present in the area proximal and distal to the catheter that is separated by the last thrombus fragments remaining in the vessel. Furthermore, it is observed that inside the catheter, the pressure values are not continuous throughout the complete catheter. At 40 ms, 80 ms and 160 ms, local pressure deviations are observed, indicated by a blue or orange area inside the catheter. The source of these local deviations is not completely clear, however one of the potential explanations could be local changes in the shape of the thrombus, allowing blood to be present or the opposite, where blood is nudged into other areas by local thrombus shape deviations. Lastly, it can be noticed that the pressure in the blood domain at t=250 ms is lower than the initially assigned blood pressure of 12 kPa. The transition to this new, lower blood pressure can be seen at t=190 ms, where a pressure difference occurs in the blood domain between the proximal and distal side of the vessel. A potential explanation for this is the removal of the thrombus volume from the vessel on the right side. Thrombus fragments obstruct the connection of the distal part of the vessel to the proximal part, where an increased pressure is located.
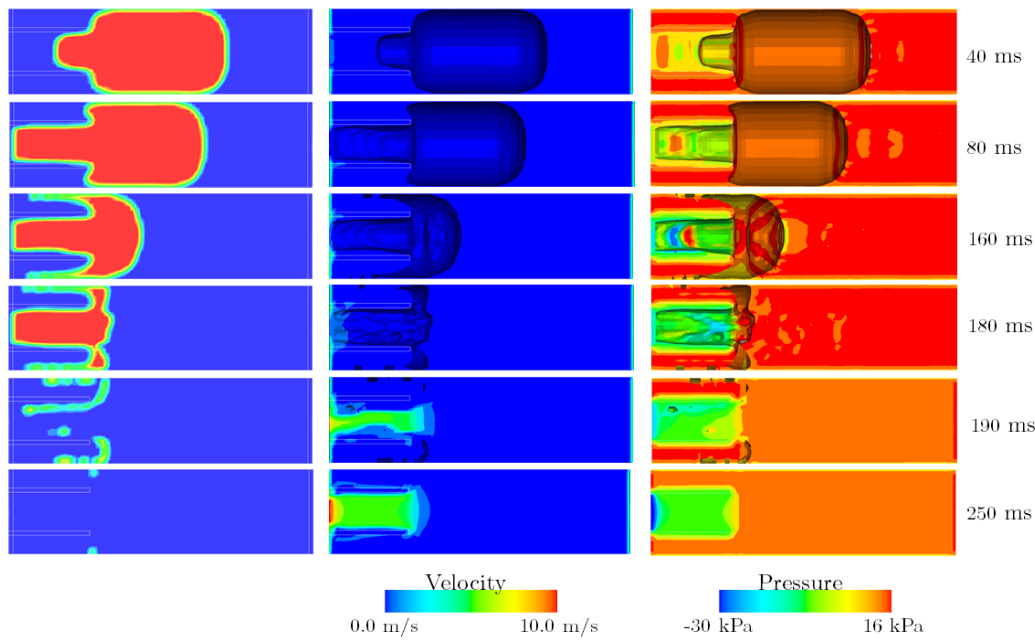
Figure 3.5: The thrombus kinematics of the Herschel-Bulkey model thrombus (left), the velocity profile during aspiration (middle) and the pressure distribution during aspiration (right) with an aspiration pressure of -30 kPa. In the velocity and pressure profile, the contour of the thrombus is shown during aspiration. The colours mapped inside this thrombus contour signify the velocity and pressure values in the blood domain behind the thrombus.

### 3.4.3. Constant Viscosity

For the constant viscosity model, the two defined viscosity values are compared, based on their thrombus kinematics. Afterwards, a detailed description is presented of the results of the higher constant viscosity model.
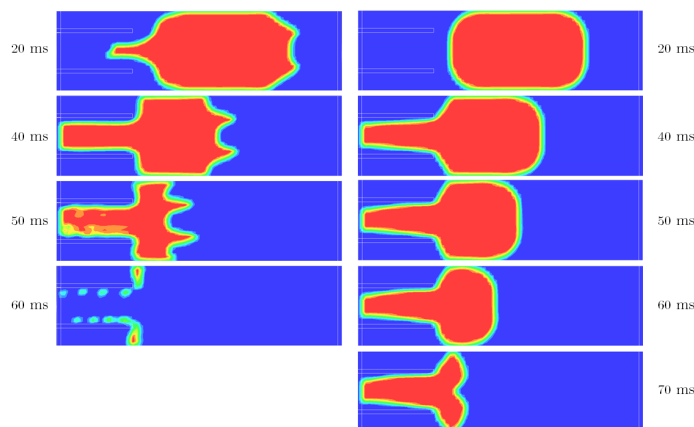


Figure 3.6: Left: The aspiration of a thrombus with a viscosity of $0.036 \frac{kg}{m.s}$ with 30 kPa aspiration pressure. Right: The aspiration of a thrombus with a viscosity of $2.15 \frac{kg}{m.s}$ with 30 kPa aspiration pressure.

In Figure 3.6, the thrombus kinematics are shown for both constant viscosity values. The difference in viscosity value for the Newtonian fluids results in a difference in both the recanalization time and thrombus shape during the aspiration. The thrombus with a higher viscosity (i.e. $2.15 \frac{kg}{m.s}$) is aspirated slower than the low viscosity thrombus (i.e. $0.036 \frac{kg}{m.s}$), where the recanalization times are 80 ms and 60 ms respectively. Together with the shape difference of the thrombus, this can be explained with the viscosity definition. The flow in the

blood domain in both models is considered to be in a similar range. However, the different viscosities imply a different resistance to flow, with a larger resistance for the thrombus with a higher viscosity. The more viscous thrombus is therefore less likely to deform when it encounters the same pressure gradient as the low viscous thrombus. This furthermore explains the longer recanalization time of the high viscous thrombus.

Figure 3.7 shows the velocity and pressure profile, together with the thrombus kinematics for the Newtonian fluid thrombus with a viscosity of $2.15\frac{kg}{m.s}$. The velocity profile is relatively similar to the Herschel-Bulkley model and power law model velocity profile, with very small velocities occurring during the aspiration itself and increased values once the thrombus is largely aspirated. The velocity profile at t=250 ms is considered to be identical to the profile of the Herschel-Bulkley model and the power law model. This could be explained by the fact that (almost) no thrombus parts remain in the vessel in all three of the cases at t=250 ms, resulting in identical physical situations. This is also the case for the pressure distribution. In accordance with the curve of the applied aspiration pressure, the absolute value of the negative pressure gradually increases, with negative pressure values primarily being located inside the catheter. The thrombus is aspirated in 80 ms, with a maximum absolute value for the negative aspiration pressure of 0.0 kPa, following the aspiration pressure application curves in Figure 2.7. Due to the higher initial pressure value of 12 kPa, which was assigned to the blood domain, the aspiration pressure is initially positive and only becomes negative after 71.5 ms.

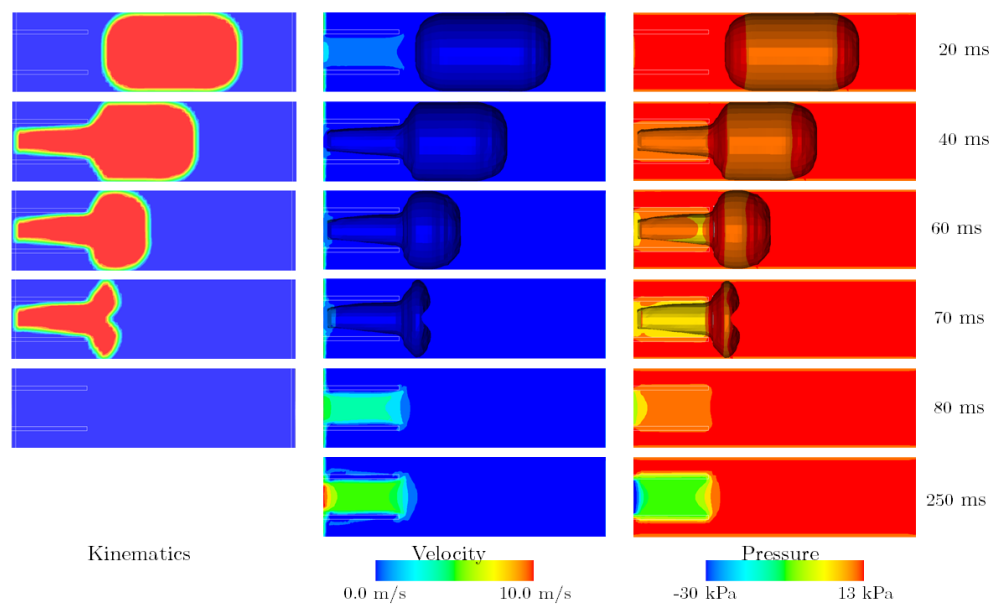

Figure 3.7: The thrombus kinematics (left), velocity profile (middle) and pressure distribution (right) for the Newtonian fluid thrombus model with a constant viscosity value of $2.15\frac{kg}{m.s}$.

## 3.5. Discussion

In the comparison of the three fluid material models, it can be observed that the thrombus behavior of the Herschel-Bulkley model and the power law model are relatively similar. However, a large difference in thrombus behavior is observable between the Newtonian fluid model and the non-Newtonian fluid models. With a recanalization time of 190 ms for the Herschel-Bulkley model, the recanalization lasts 10 ms longer than the recanalization of the power law model thrombus and more than double the recanalization time of the constant viscosity (i.e. 80 ms). With regards to the thrombus behavior during aspiration, it is noticeable that segments of the thrombus move into the proximal area between the catheter and vessel wall for both non-Newtonian fluid models. These segments extend to a more proximal location tip and comprise of a larger volume for the Herschel-Bulkley model than the thrombus parts of the power law model. Contrary to the non-Newtonian fluid models, no thrombus segments move into the area between the catheter and the vessel wall when the Newtonian fluid model is used.

The similarity of the thrombus behavior of the Herschel-Bulkley and power law model can be explained by their foundation on a power law equation (see Equation 3.2 and 3.1) albeit in different forms. The linear shear stress-shear strain relation for the Newtonian fluid, contrary to the non-linear relationship for the non-Newtonian fluids could partially explain the distinction in thrombus behavior. For future research, it could be insightful to introduce a different material model that connects the solid and fluid phase. An example of this could be the Bingham fluid, that applies a constant viscosity once the yield stress is passed and thus does not make use of a power law equation. [44] This could be a new form of combining the solid and fluid phase into one material model.

Based on the theory behind the Herschel-Bulkley model, it was expected that different strains would occur than those of the power law model, especially during the initial phase of the aspiration with increasing stresses. This was not the case, with very similar strains to the power law model. Furthermore, when comparing different material parameter sets (i.e. LYS and HYS), almost identical strains occur, with the exception of the 20 ms before complete recanalization. This deviated from the anticipated thrombus behavior, where different strains were expected for identical stresses. According to the definition of the model, a higher yield stress should enlarge the stress range of the solid phase. In the application of increasing yield stresses, a higher yield stress did not result in a distinguishable solid phase that was recognized during the thrombus aspiration. However, the comparison of first principle stresses of both parameter sets demonstrate a difference between both thrombi, with higher stresses for the HYS thrombus compared to the LYS thrombus. It can thus be concluded that similar strains occur for identical applied pressures, yet larger stresses inside the thrombus exist for a material parameter set with a larger yield stress. Very little documentation or previous work is found concerning the Herschel-Bulkley model in LS-DYNA [29]. The discrepancy between the expected thrombus behavior and the results could thus be evoked by an uncomplete implementation of the material model in the software or by a misguided interpretation of the material model. Nevertheless, in the made observations of the results, no distinguishable solid phase was recognized during the thrombus aspiration.

Lastly, it is observed that the thrombus behavior for the Newtonian fluid model differs largely for the different $\mu$ values. Not only does it change the recanalization time, it also largely changes the thrombus shape during aspiration. Since different $\mu$ values give very different outcomes, it is of utmost importance to define the viscosity value very carefully. Beside the used viscosity value of $0.036 \frac{kg}{m.s}$ based on Pennati *et al.* [23], no constant

viscosity values for thrombi were found in literature. It would therefore be advised to conduct viscosity mea-surements in the future to try to estimate a viscosity value for a certain thrombus composition. Nevertheless, it should be considered that thrombi exhibit both fluid and solid behavior and that its material properties can thus never fully be captured in one viscosity value.

### 3.5.1. Limitations

One of the limitations of this study is that there is no ground for comparison of the thrombus material models with real thrombi. The overarching goal of comparing three different fluid material models is to mimic the medical situation as close as possible. However, it was not within the scope of this project to compare the situation in the model with retrieved or analog thrombi. It is thus not possible to state anything about the resemblance between the fluid models and actual thrombus behavior. Comparing the modelled thrombus behavior with real thrombus behavior is a crucial part in the path towards realistic thrombus material mod-els. It would therefore be a great next step in the path towards realistic thrombus models to compare the two in future research.

Secondly, it should be noted that the different material models don't describe the same thrombus. Each of the material models has its own input parameters, which were defined separately, portraying three different thrombi. Describing one specific thrombus using the three different fluid material models was not possible, because it required the corresponding material parameters for each specific model. As mentioned in Chapter 1, patient-retrieved thrombi largely vary in composition and mechanical properties. No set of material pa-rameters that accurately describes a "generic" thrombus can be generated, because a generic thrombus does not exist. However, comparing the three fluid material models gives relevant insights into how these models depict thrombus behavior. Due to the large differences, it is likely that one material model resembles the be-havior of a range of thrombi more closely than another material model. An example of this is the movement of thrombus into the area between the catheter and the vessel wall in the power law model and the Herschel-Bulkley model, which is not the case in the constant viscosity model. This is very specific behavior that might or might not resemble thrombus behavior during aspiration accurately. In line with previous recommenda-tions, it would be interesting to investigate the relationship between the modelled thrombus behavior and patient-retrieved thrombus behavior in future research.

Lastly, by using a fluid material model for the thrombus, this work partly overlooks the solid material prop-erties of thrombi. Other than the Herschel-Bulkley model that incorporates solid-like behavior, the solid ma-terial properties are not included in the material models. Thrombi exhibit both solid and fluid behavior [43] and discarding one of either undervalues the particular thrombus properties. A potential future advancement would be to compare fluid thrombus models to the existing [14], [15], [17] or new solid thrombus models. A consecutive comparison to patient retrieved thrombi would be the crucial next step in order to analyze their resemblance in the path towards realistic thrombus material models.

# 4

# Clinical parameters

The future goal of computational aspiration thrombectomy research is to improve the medical practice by giving relevant insight into the procedure. Furthermore, it could possibly give information about patient-specific or adjustable parameters and their influence on the thrombectomy outcome. Therefore, three adjustable or patient-specific parameters that are deemed relevant for the medical practice were chosen to vary in this thesis: aspiration pressure, aspiration distance and thrombus length. Each of these parameters had three variations to compare the results. The model that functioned as the baseline for this part of the research included an aspiration pressure of 50 kPa, a suction distance of 2.0 mm, a thrombus length of 5.0 mm and a Herschel-Bulkley thrombus material model with the material parameters used in Chapter 3. The Herschel-Bulkley material model was opted for because of its (theoretical) integration of solid and fluid material properties in one material model, resembling the nature of patient-retrieved thrombi.[25]

The variation of clinical parameters is evaluated based on their respective recanalization time. The total recanalization time is divided in two parts, the time where the thrombus is still completely outside of the catheter and the time where the thrombus, or a part of it is inside the catheter. The outcome parameter of recanalization time was opted for, since it can be measured during the medical procedure as well, alongside the fact that it allows to make conclusions and advice related to the procedure outcome.

## 4.1. Aspiration Pressure

The investigation of the aspiration pressure is relevant for the clinical practice, since it is an adaptable setting in the procedure. The range of applied aspiration pressures in literature extends from 10 kPa to 100 kPa. In order to investigate its influence to the full extent, the three chosen aspiration pressure values are 10, 50 and 100 kPa. The applied aspiration pressures follow a similar linear curve, starting at 0 kPa and reaching the respective aspiration pressure at t=250 ms, similar to the curves shown in Figure 2.7 in Chapter 2.

33

Table 4.1: The three variations for the clinical parameter of the aspiration pressure.

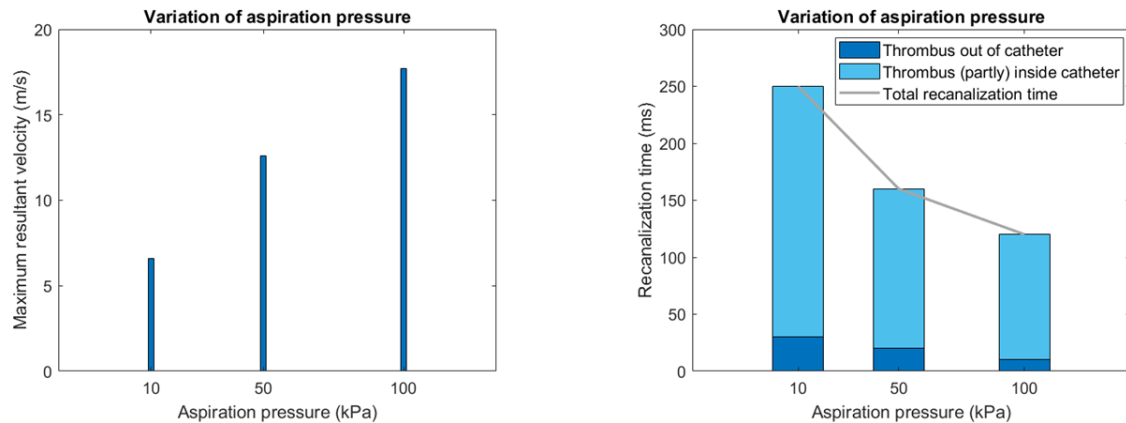|                          | *Model 1* | *Model 2* | *Model 3* |
|--------------------------|-----------|-----------|-----------|
| **Aspiration pressure (kPa)** | 10        | 50        | 100       |

### 4.1.1. Results



Figure 4.1: The maximum resultant velocities (left) for aspiration pressures of 10, 50 and 100 kPa and the recanalization time (right)

The maximum resultant velocity present in the models, together with the resultant recanalization times for the three aspiration pressures is shown in Figure 4.1. It can be observed that the maximum resultant velocity for 100 kPa is almost three times the maximum resultant velocity for 10 kPa, with 17.7 m/s and 6.6 m/s respectively. The recanalization time decreases largely for increasing aspiration pressures, with a total difference between 10 and 50 kPa of 90 ms and a total difference between 50 and 100 kPa of 40 ms. The relation between total recanalization time and aspiration pressure is thus not linear. The total recanalization time of 100 kPa is less than half the total recanalization time of 10 kPa, with 120 ms and 250 ms respectively. The separate recanalization times (i.e. the thrombus is out or (partly) inside the catheter) all decrease for increasing aspiration values. The recanalization time where the thrombus is completely out of the catheter is linear, with a decrease of 10 ms between each aspiration pressure value.

## 4.2. Suction Distance

In literature, no general consensus has been reached concerning the perfect suction distance between the catheter tip and the thrombus. Since the chosen value for the suction distance in the GW model is 2 mm, it is opted to deviate from this distance with 1.0 mm, resulting in the following suction distances: 1.0 mm, 2.0 mm and 3.0 mm. It was chosen not to model direct contact, since this might cause fragmentation of the thrombus according to Talayero *et al.* [14]. Investigating the impact of direct contact is considered to be another research scope, although it is an interesting topic. In order to investigate the influence of suction distance on the recanalization time without the influence of another factor, it was decided not to model direct contact.

Suction distance is also a parameter that can vary in the medical procedure. Although it might be a heavy demand for the interventionalist executing the thrombectomy to adjust the suction distance to the exact advised

distance in millimeters, the research into the influence of suction distance on recanalization could deliver insightful advice on the importance of suction distance. Its priority could then potentially be reconsidered in the trade-off between precision and time during the procedure.

Table 4.2: The three variations for the clinical parameter of the suction distance.

|                          | *Model 1* | *Model 2* | *Model 3* |
|--------------------------|-----------|-----------|-----------|
| **Suction distance (mm)** | 1.0       | 2.0       | 3.0       |

## 4.2.1. Results
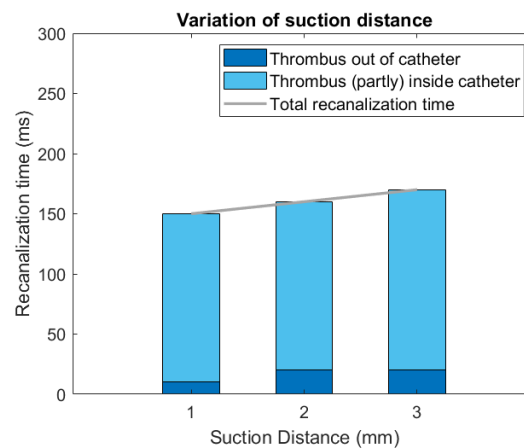


Figure 4.2: The recanalization time for suction distances of 1.0 , 2.0 and 3.0 mm.

The total recanalization time for the different suction distances is shown in Figure 4.2. With a total recanalization time of 150 ms for 1.0 mm suction distance, 160ms for 2.0 mm suction distance and 170 ms for 3.0 mm suction distance, the total recanalization time increases linearly, with an increment of 10 ms for a suction distance increment of 1.0 mm. However, the separate recanalization times where the thrombus is out of the catheter or (partly) inside the catheter do not show a clear relation yet. For each suction distance variation, one of the separate recanalization times remains constant, whereas the other separate recanalization time increases. The recanalization time where the thrombus is out of the catheter is 10, 20 and 20 ms for suction distances of 1.0, 2.0 and 3.0 mm. The accompanying recanalization times when the thrombus is (partly) inside the catheter is 140, 140 and 150 ms respectively.

## 4.3. Thrombus Length

The third clinical parameter that is investigated is thrombus length. Because thrombi properties and dimensions are patient-specific, a variation is present in the medical practice. In order to investigate the influence of this patient-specific parameter on the outcome of the aspiration thrombectomy, its value was varied. Contrary to the previous two parameters, this parameter is unalterable during the procedure and therefore out of the medical team's hands. However, information on the influence of thrombus length on the procedure outcome could allow the medical team to anticipate and adapt other parameters (e.g. suction distance, aspiration pressure) in order to achieve the best possible treatment outcome. With a baseline value for the thrombus length of 5.0 mm, a deviation was opted for of 2.0 mm. This results in the following thrombus lengths: 3.0 mm, 5.0 mm and 7.0 mm. All thrombus lengths were placed inside the model to have a suction distance of 2.0 mm to the catheter.

Table 4.3: The three variations for the clinical parameter of the thrombus length.

|  | *Model 1* | *Model 2* | *Model 3* |
|---|---|---|---|
| **Thrombus length (mm)** | 3.0 | 5.0 | 7.0 |

### 4.3.1. Results
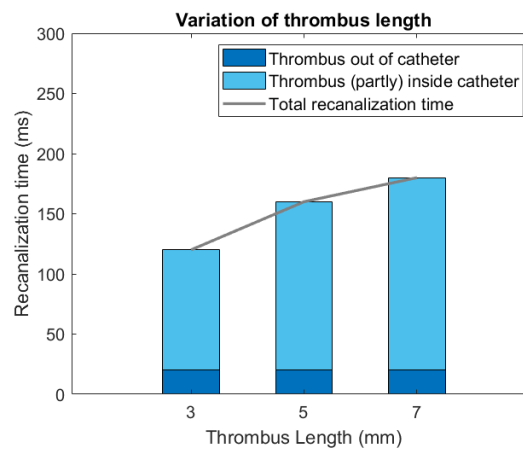


Figure 4.3: The recanalization time for suction distances of 1.0 , 2.0 and 3.0 mm.

In Figure 4.3, the recanalization time for the different thrombus lengths can be seen. The recanalization time increases for increasing thrombus lengths. The difference in recanalization time between the 3.0 mm and 5.0 mm thrombus was 40 ms, which is double the time difference between the 5.0 and 7.0 mm thrombus (i.e. 20 ms). Along with the clinical parameter of the aspiration pressure, the relationship between the recanalization time and the thrombus length is not linear. The recanalization time where the thrombus is completely outside of the catheter (i.e. the thrombus is moving towards the catheter) remains at a constant value of 20 ms for all three thrombus lengths. The recanalization time where the thrombus was located (partly) inside the catheter was 100, 140 and 160 ms for the increasing thrombus lengths.

# 4.4. Discussion

### 4.4.1. Aspiration Pressure

It can be observed that the decrease in recanalization time for higher absolute aspiration pressure values is not linear. The decrease of recanalization time of 90 ms between 10 and 50 kPa is larger than the decrease of 40 ms between 50 and 100 kPa. These results are in accordance with the trend for increasing aspiration pressures in the study of Soleimani *et al.* [16], where the decrease in recanalization time between 15 and 40 kPa is relatively large, compared to the decrease for aspiration pressures between 40 and 60 kPa. This non-linearity suggests that there might be an aspiration pressure threshold value above which the reduction in recanalization time is negligible.

In the comparison with the results of Soleimani *et al.* [16], it is observable that the order of magnitude of recanalization time is quite different, with a recanalization time of 3s for an aspiration pressure of 50 kPa, compared to 160 ms in this model. This has already been discussed in Chapter 2, Section 2.7 and could be subject to future research.

A downside to consider, is the fact that aspiration pressure values can potentially damage the vessel wall [17] and therefore the aspiration pressure can't be increased infinitely. According to Soleimani *et al.* [16], the maximum tolerable pressure value for vessels is 100 kPa, based on the study of Romero *et al.* [18]. Talayero *et al.* [17] define 80 kPa as the highest pressure value without causing potential vessel damage, yet no foundation is given for this statement. No other literature concerning aspiration thrombectomies was found to support or refute these maximum pressure values and to describe the potentially caused vessel damage. A similar circumstance (i.e. a negative pressure exerted by a catheter inside a vessel) occurs when blood is extracted through an intravenous catheter. In the analysis of Mrazek *et al.* [45], the applied negative pressures ranges from 6.1 psi to 12.0 psi, which is 42.06 kPa and 82.74 kPa respectively. No occurrence of vessel rupture was reported in this analysis. These values are in a similar range as the applied negative pressure values during aspiration thrombectomy. The earlier mentioned maximum aspiration pressure values are moreover conform with the applied pressures during blood collection and thus seem realistic. Further research into vessel rupture due to negative pressure is advised to include this into future models.

Based on this information, the advice to the interventionalist would be to use an aspiration pressure that is preferably as high as possible. The upper threshold could be assumed to be 100 kPa, yet future research might establish another pressure value. Determining the relation between recanalization time and aspiration pressure in a more specific way, with a focus on a this potential aspiration pressure threshold, would be an advised topic for future research.

### 4.4.2. Suction Distance

The relation between the suction distance and the total recanalization time seems to be linear, based on the current simulations. Despite this linearity, no clear relationship can be drawn between the variation of suction distance and the separate recanalization times where the thrombus is inside or out of the catheter. This is due to the fact that both of the separate recanalization times (i.e. thrombus in or out of the catheter) remain constant for one deviation in the suction distance and vary for another one. It is therefore only possible to deliver a statement concerning the relation between the total recanalization time and the variation of suction

distance during the aspiration thrombectomy. Larger suction distances result in higher recanalization time and a suction distance as little as possible is thus advised.

Due to computational load restraints, no larger suction distances were modelled. Compared to the other clinical parameters, the recanalization time improvement of 10 ms for an added 1.0 mm of suction distance is considered to be relatively small. However, in the evaluation of the relatively small difference in recanalization times for the three suction distances, it should be considered that the variation is in the order of millimeters. In the developed model this is a relatively large difference, yet in the medical practice it might be difficult to be precise to this extent, given the fact that the interventionalist needs to execute this procedure based on medical imaging. If the found linear relation is assumed to be applicable for all suction distances, the difference in recanalization time between a suction distance of e.g. 5.0 mm and 1.0 mm could result in a considerably quicker recanalization. In this case, the difference would be assumed to be 40 ms.

Future research is advised for the relation between suction distance and recanalization time. First of all, future research with a larger variation of suction distances is advised to understand the relation better and investigate the linearity of it for larger and smaller suction distances. Secondly, it is advised to perform research into the aspiration of the thrombus for a suction distance of 0.0 mm, implying there is direct contact between the thrombus and the catheter tip. Whether or not direct contact is favourable is a topic of disagreement between various authors. On the one hand, supporters of direct contact [19], [46] are convinced that it stimulates a better recanalization. The opponents of direct contact [14] on the other hand, state that it might cause thrombus fragmentation. Based on the performed simulations, no statements can be made regarding direct contact and its link with thrombus fragmentation. Nevertheless, more extensive research needs to be performed in order to draw definite conclusions.

### 4.4.3. Thrombus Length

Considering the identical recanalization times when the thrombus is (partly) inside the catheter, it can be concluded that different thrombus lengths affect the aspiration primarily once the thrombus is already inside the catheter. In the comparison of these specific recanalization times (i.e. once the thrombus is partly inside the catheter), it can be concluded that the difference in recanalization time is halved. The relation is therefore considered to be non-linear. If it is assumed that this relation extends for all thrombus lengths, the recanalization time is likely to reach a plateau, where a larger thrombus length does not result in a much longer recanalization time. This plateau might be reached at a smaller thrombus length than the average of 18.0 mm [33]. This would imply that at this average, no considerable changes would occur in the recanalization time for larger or smaller thrombi.

The relatively small lengths of the modelled thrombi can be considered to be a limitation of this study. However, a broad range of thrombus lengths exists in patients, deviating from its average value of 18.0 mm [33]. A more extensive study with a larger range of thrombus lengths is advised into the relation between thrombus length and aspiration time, based on the difference with the average thrombus length of 18.0 mm, together with the non-linearity of the observed relation and the question whether this relation is applicable for most of the thrombus lengths.

### 4.4.4. General Discussion

Generally, it can be stated that all three of the parameters influence the recanalization time. Within the capacity of this model, each parameter could be varied to a different extent. This resulted in variations of a few millimeters for the suction distance and thrombus length due to the computational load, and larger variations for the aspiration pressure (i.e. 40 and 50 kPa). For the evaluated ranges, it can be concluded that the variation of aspiration pressure has the largest influence on the recanalization time. Nevertheless, if the other two parameters can be varied to a larger extent, their influence could potentially be somewhat similar. All three clinical parameters and their found relations with recanalization time can act as the foundation for new research questions in future studies.

# 5

# Conclusion

In this thesis, a computational aspiration thrombectomy model was developed, applying a fluid material model to the thrombus. This goal was considered to be achieved successfully, with a working model where a thrombus was aspirated due to a negative aspiration pressure. The applied aspiration pressure generated very high velocities inside the catheter and a steep decrease in velocity at the tip of the catheter. The application of three different fluid material models resulted in a distinction in thrombus behavior between the Newtonian fluid material model and the non-Newtonian fluid material models (i.e. power law and Herschel-Bulkley model). The Herschel-Bulkley model performed differently than expected, with no differentiation between material parameter sets of separate yield stresses. A crucial next step would be the verification of the thrombus material models, by utilizing clot analogs or patient-retrieved thrombi. The evaluation of the influence of three clinical parameters (i.e. aspiration pressure, suction distance and thrombus length) on the recanalization time, showed a relationship for each clinical parameter yet needs to be investigated more deeply. This new computational aspiration thrombectomy model has delivered useful information that allows various propositions for future research to be formulated, for both clinical and technical perspectives.

# A

# Simulation Code

In this Appendix, the code is added for the Model used in Chapter 4, with an **aspiration pressure of -50 kPa, 2.0 mm suction distance, a thrombus length of 5.0 mm and the Herschel-Bulkley material model with a** $\sigma_0 = 0.035 MPa$. This is the reduced input file, without the node list in order to create a relatively compact appendix.

```
$# LS-DYNA Keyword file created by LS-PrePost(R) V4.8.11 - 22Feb2021
*KEYWORD
*TITLE
$#                                                                    title
LS-DYNA keyword deck by LS-PrePost
*CONTROL_ACCURACY
$#       osu       inn    pidosu      iacc
           1         1         0         0
*CONTROL_ALE
$#       dct      nadv      meth      afac      bfac      cfac      dfac      efac
          -1         1         2      -1.0       0.0       0.0       0.0       0.0
$#     start       end     aafac     vfact      prit       ebc      pref   nsidebc
        0.01.00000E20        1.01.00000E-6         1         0       0.0         0
$#      ncpl      nbkt    imascl    checkr    beamin   mmgpref    pdifmx   dtmufac
           1        50         0       0.0       0.0         0       0.0       0.0
$# optimpp    ialedr    bndflx    minmas
           0         0        01.00000E-5
*CONTROL_BULK_VISCOSITY
$#        q1        q2      type     btype    tstype
         1.5      0.06         1         0         0
*CONTROL_ENERGY
$#      hgen      rwen    slnten     rylen     irgen
           2         2         2         2         2
```

*CONTROL_MPP_DECOMPOSITION_DISTRIBUTE_ALE_ELEMENTS
*CONTROL_TERMINATION

| $# | endtim | endcyc | dtmin | endeng | endmas | nosol |
|---|---|---|---|---|---|---|
| | 250.0 | 0 | 0.0 | 0.01 | .000000E8 | 0 |

*CONTROL_TIMESTEP

| $# | dtinit | tssfac | isdo | tslimt | dt2ms | lctm | erode | ms1st |
|---|---|---|---|---|---|---|---|---|
| | 0.0 | 0.9 | 0 | 0.0 | -1.0000E-4 | 0 | 0 | 0 |

| $# | dt2msf | dt2mslc | imscl | unused | unused | rmscl | unused | ihdo |
|---|---|---|---|---|---|---|---|---|
| | 0.0 | 0 | 0 | | | 0.0 | | 0 |

*DATABASE_GCEOUT

| $# | dt | binary | lcur | ioopt |
|---|---|---|---|---|
| | 5.0 | 0 | 0 | 1 |

*DATABASE_GLSTAT

| $# | dt | binary | lcur | ioopt |
|---|---|---|---|---|
| | 5.0 | 0 | 0 | 1 |

*DATABASE_MATSUM

| $# | dt | binary | lcur | ioopt |
|---|---|---|---|---|
| | 5.0 | 0 | 0 | 1 |

*DATABASE_BINARY_D3PLOT

| $# | dt | lcdt | beam | npltc | psetid |
|---|---|---|---|---|---|
| | 10.0 | 0 | 0 | 0 | 0 |

| $# | ioopt | rate | cutoff | window | type | pset |
|---|---|---|---|---|---|---|
| | 0 | 0.0 | 0.0 | 0.0 | 0 | 0 |

*DATABASE_BINARY_FSIFOR

| $# | dt | lcdt | beam | npltc | psetid | cid |
|---|---|---|---|---|---|---|
| | 10.0 | 0 | 0 | 0 | 0 | 0 |

*DATABASE_EXTENT_BINARY

| $# | neiph | neips | maxint | strflg | sigflg | epsflg | rltflg | engflg |
|---|---|---|---|---|---|---|---|---|
| | 0 | 0 | 3 | 0 | 1 | 1 | 1 | 1 |

| $# | cmpflg | ieverp | beamip | dcomp | shge | stssz | n3thdt | ialemat |
|---|---|---|---|---|---|---|---|---|
| | 0 | 0 | 0 | 1 | 1 | 1 | 2 | 1 |

| $# | nintsld | pkp_sen | sclp | hydro | msscl | therm | intout | nodout |
|---|---|---|---|---|---|---|---|---|
| | 0 | 0 | 1.0 | 0 | 0 | 0 | | |

| $# | dtdt | resplt | neipb | quadr | cubic |
|---|---|---|---|---|---|
| | 0 | 0 | 0 | 0 | 0 |

*BOUNDARY_SPC_SET_ID

| $# | id | | | | | | | heading |
|---|---|---|---|---|---|---|---|---|
| | 1 | Fixation vessel | | | | | | |

| $# | nsid | cid | dofx | dofy | dofz | dofrx | dofry | dofrz |
|---|---|---|---|---|---|---|---|---|
| | 1 | 0 | 1 | 1 | 1 | 1 | 1 | 1 |

*SET_NODE_LIST_TITLE
fix_fluid

| $# | sid | da1 | da2 | da3 | da4 | solver |
|---|---|---|---|---|---|---|

```
         1         0.0        0.0        0.0        0.0MECH
$#     nid1       nid2       nid3       nid4       nid5       nid6       nid7       nid8
*BOUNDARY_SPC_SET_ID
$#       id                                                              heading
         1z
$#     nsid        cid       dofx       dofy       dofz      dofrx      dofry      dofrz
         3          0          0          0          1          1          1          0
*SET_NODE_LIST_TITLE
z_symm
$#      sid        da1        da2        da3        da4     solver
         3         0.0        0.0        0.0        0.0MECH
$#     nid1       nid2       nid3       nid4       nid5       nid6       nid7       nid8

*SECTION_SOLID_TITLE
PSOLID
$#    secid      elform        aet     unused     unused     unused     cohoff     unused
         6          1          0                                             0
*SECTION_SOLID_TITLE
Default PSOLID Property
$#    secid      elform        aet     unused     unused     unused     cohoff     unused
         9          1          0                                             0
*SECTION_SHELL_TITLE
Thrombus full occlusion_body1
$#    secid      elform       shrf        nip      propt     qr/irid      icomp      setyp
        11          2        1.0          2        1.0          0          0          1
$#       t1         t2         t3         t4       nloc      marea       idof     edgset
        1.0        1.0        1.0        1.0        0.0        0.0        0.0          0
*SET_PART_LIST_TITLE
Blood
$#      sid        da1        da2        da3        da4     solver
         1         0.0        0.0        0.0        0.0MECH
$#     pid1       pid2       pid3       pid4       pid5       pid6       pid7       pid8
         1          3          6          7          0          0          0          0
*SET_SEGMENT_TITLE
Aspi_segment
$#      sid        da1        da2        da3        da4     solver
         1         0.0        0.0        0.0        0.0MECH
$#       n1         n2         n3         n4         a1         a2         a3         a4

*SET_SEGMENT_TITLE
vessel_ICA
$#      sid        da1        da2        da3        da4     solver
         2         0.0        0.0        0.0        0.0MECH
```

```
$#        n1          n2          n3          n4          a1          a2          a3          a4


*SET_SEGMENT_TITLE
vessel_MCA
$#       sid         da1         da2         da3         da4      solver
           3         0.0         0.0         0.0         0.0MECH

$#        n1          n2          n3          n4          a1          a2          a3          a4


*END
```

# B

# Additional Herschel-Bulkley model

During this work, an additional material parameter set was generated for the Herschel-Bulkley model. This parameter set resulted in a yield stress $\sigma_0 = 0.025 MPa$. The chosen parameters were the following: $\tau_0 = 0.02$ and $\dot{\gamma}_c = 0.3$ .
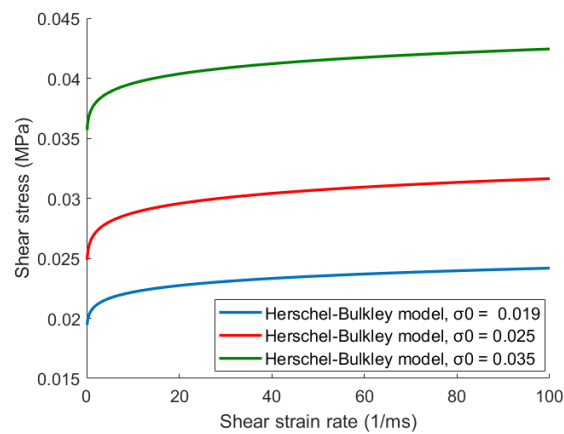


Figure B.1: The shear stress-shear strain rate relation for the three parameter sets. (The additional one is shown in red)
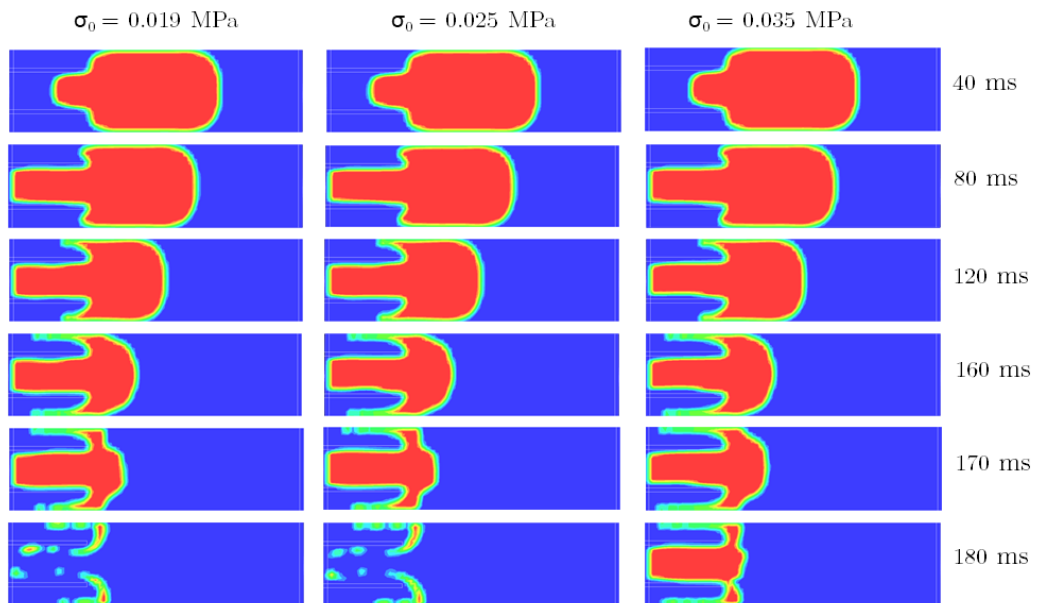
# B.1. Results



Figure B.2: The thrombus kinematics for all three parameter sets.
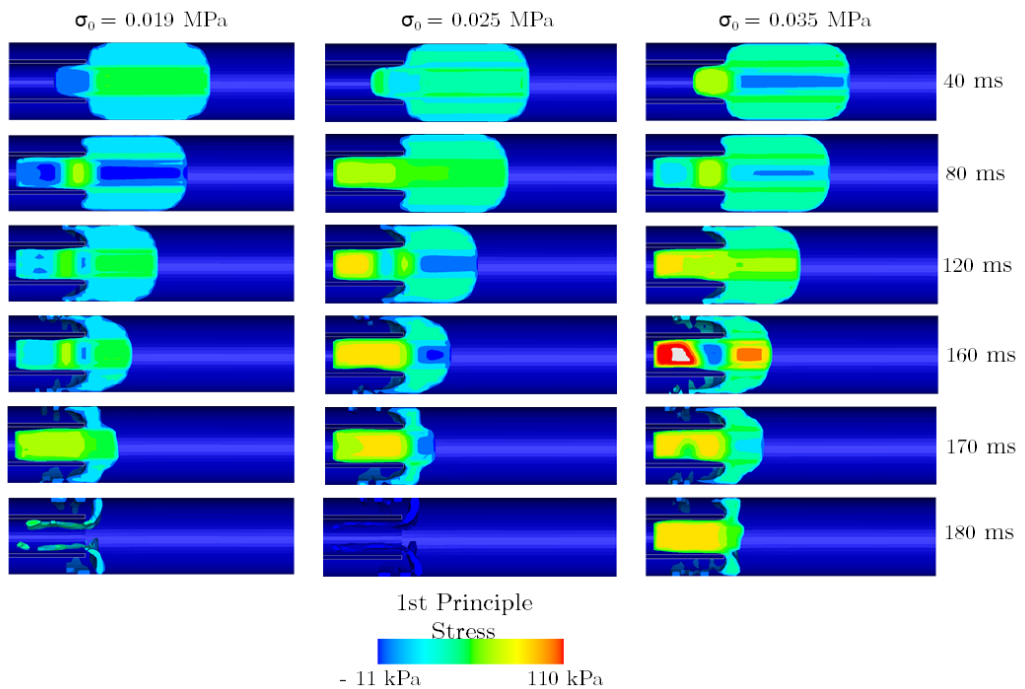


Figure B.3: The first principle stresses for all three parameter sets.

# C

# Additional Power Law model

In the study of Soleimani *et al.* [16], three different power law curves are applied. In this thesis, only the low viscous (LV) thrombus is shown. However, all three viscosity curves were modelled and applied. The respective values for Equation 3.1 are shown in Table C.1

Table C.1: *K* and *n* values based on Soleimani *et al.* [16]

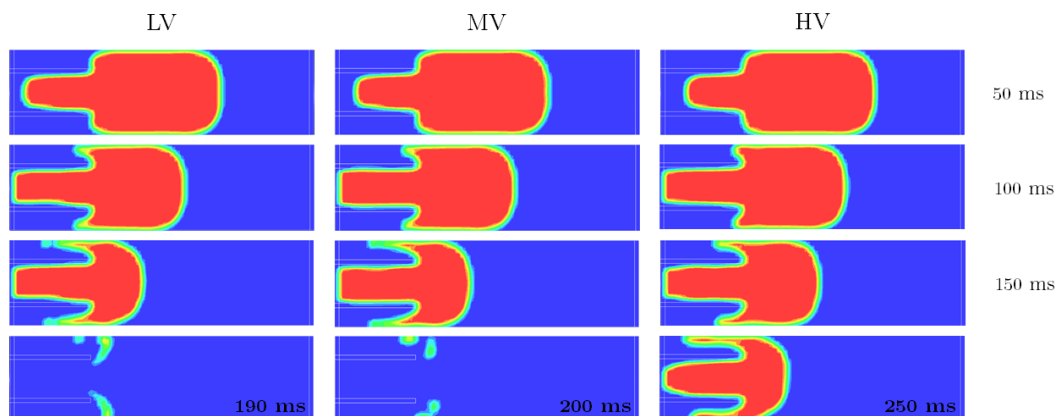| Thrombus | $K$ | $n$ |
|---|---|---|
| Low viscosity (LV) | 0.02145 | 0.1134 |
| Medium viscosity (MV) | 0.03414 | 0.0812 |
| High viscosity (HV) | 0.09865 | 0.0448 |

## C.1. Results



Figure C.1: The thrombus kinematics for all the three powerlaw viscosity curves.

# D

## Overview simulations

All the performed simulations for this project will be available for future students at the Lab at Erasmus MC through the transfer of documents. An overview of the final models that were executed:

- GW Model

  - GW model for the following aspiration pressures : 10, 30, 50, 70 and 100 kPa

- GWB Model

  - GWB model for the following aspiration pressures : 10, 30, 50, 70 and 100 kPa

- Constant viscosity model

  - Viscosity value $0.036 \frac{kg}{m.s}$
  - Viscosity value $2.15 \frac{kg}{m.s}$

- Power law viscosity model

  - Low viscosity power law

  - Medium viscosity power law

  - High viscosity power law

- Herschel-Bulkley model

  - Yield stress 0.019 MPa

  - Yield stress 0.025 MPa

  - Yield stress 0.035 MPa

- Variation aspiration pressure : 10 , 50, 100 kPa

- Variation suction distance: 1, 2, 3 mm

- Variation thrombus length: 3, 5, 7 mm

Additional models that would potentially be interesting for future students :

- Variation of density and viscosity separately for the constant viscosity model

- Mesh sensitivity study

# Bibliography

[1]  World Health Organization, "Acute Stroke - Background Paper," no. October, 2004.

[2]  S. A. Smith, R. J. Travers, and J. H. Morrissey, "How it all starts: Initiation of the clotting cascade," *Critical Reviews in Biochemistry and Molecular Biology*, vol. 50, no. 4, pp. 326–336, 2015. DOI: 10.3109/10409238.2015.1050550.

[3]  J. L. Saver, "Time is brain - Quantified," *Stroke*, vol. 37, no. 1, pp. 263–266, 2006. DOI: 10.1161/01.STR.0000196957.55928.ab.

[4]  D.-h. Kang, J. Park, and D. Ph, "Endovascular Stroke Therapy Focused on Stent Retriever Thrombectomy and Direct Clot Aspiration : Historical Review and Modern Application," vol. 60, no. 3, pp. 335–347, 2017.

[5]  A. J. Yoo, "Thrombectomy in Acute Ischemic Stroke : Challenges to Procedural Success," vol. 19, no. 2, pp. 121–130, 2017.

[6]  J. A. Grossberg *et al.*, "Beyond Large Vessel Occlusion Strokes," pp. 1662–1668, 2018. DOI: 10.1161/STROKEAHA.118.020567.

[7]  J. Mocco *et al.*, "Aspiration Thrombectomy After Intravenous Alteplase Versus Intravenous Alteplase Alone," pp. 2331–2338, 2016. DOI: 10.1161/STROKEAHA.116.013372.

[8]  J. M. Ospel *et al.*, "Optimizing fast first pass complete reperfusion in acute ischemic stroke – the BADDASS approach ( BAlloon guiDe with large bore Distal Access catheter with dual aspiration with Stent-retriever as Standard approach )," *Expert Review of Medical Devices*, vol. 00, no. 00, pp. 1–9, 2019. DOI: 10.1080/17434440.2019.1684263.

[9]  Z. Vardar *et al.*, "Biomechanics and hemodynamics of stent-retrievers," 2020. DOI: 10.1177/0271678X20916002.

[10] P. R. Konduri *et al.*, "In-Silico Trials for Treatment of Acute Ischemic Stroke," vol. 11, no. September, pp. 1–8, 2020. DOI: 10.3389/fneur.2020.558125.

[11] F. Migliavacca, "Is modeling stents still an important issue?" *Procedia Structural Integrity*, vol. 15, pp. 46–50, 2019. DOI: 10.1016/j.prostr.2019.07.009.

[12] F. R. I. Annaccone *et al.*, "Computer Simulations in Stroke Prevention : Design Tools and Virtual Strategies Towards Procedure Planning," vol. 4, no. 4, pp. 291–308, 2013. DOI: 10.1007/s13239-013-0134-x.

[13] A. Angermaier and S. Langner, "Recanalization and Reperfusion in Acute Stroke - More Often Different than Alike," *Clinical Neuroradiology*, vol. 26, no. 3, pp. 375–376, 2016. DOI: 10.1007/s00062-015-0470-3.

[14] C. Talayero *et al.*, "Thrombectomy aspiration device geometry optimization for removal of blood clots in cerebral vessels," vol. 14, no. 1, pp. 6229–6237, 2020.

[15] A. Chitsaz and A. Nejat, "Three-Dimensional Numerical Simulations of Aspiration Process : Evaluation of Two Penumbra Aspiration Catheters Performance," no. 7, 2018. DOI: 10.1111/aor.13300.

[16] S. Soleimani, G. Dubini, and G. Pennati, "Performance of a thrombectomy device for aspiration of thrombus with various sizes based on a computational fluid dynamic modeling," 2015. DOI: 10.1515/bmt-2014-0013.

[17] C. Talayero *et al.*, "Numerical modelling of blood clot extraction by aspiration thrombectomy . Evaluation of aspiration catheter geometry," *Journal of Biomechanics*, vol. 94, pp. 193–201, 2019. DOI: 10.1016/j.jbiomech.2019.07.033.

[18] G. Romero *et al.*, "Modelling and simulation of a thrombectomy probe applied to the middle cerebral artery by using the bond graph technique," *Spring Simulation Multiconference 2010, SpringSim'10*, pp. 1–8, 2010. DOI: 10.1145/1878537.1878768.

[19] Y. Shi *et al.*, "Physics in Medicine Suction force-suction distance relation during aspiration thrombectomy for ischemic stroke : A computational fl uid dynamics study," *Physics in Medicine*, vol. 3, pp. 1–8, 2017. DOI: 10.1016/j.phmed.2016.11.001.

[20] I. G. Jansen, M. J. Mulder, and R. J. B. Goldhoorn, "Endovascular treatment for acute ischaemic stroke in routine clinical practice: Prospective, observational cohort study (MR CLEAN Registry)," *BMJ (Online)*, vol. 360, 2018. DOI: 10.1136/bmj.k949.

[21] G. Romero *et al.*, "Modeling of blood clot removal with aspiration Thrombectomy devices," vol. 14, no. 1, pp. 6238–6250, 2020.

[22] B. C. Good *et al.*, "Development of a computational model for acute ischemic stroke recanalization through cyclic aspiration," *Biomechanics and Modeling in Mechanobiology*, vol. 19, no. 2, pp. 761–778, 2020. DOI: 10.1007/s10237-019-01247-w.

[23] G. Pennati *et al.*, "Numerical Simulation of Thrombus Aspiration in Two Realistic Models of Catheter Tips," vol. 34, no. 4, pp. 301–310, 2010. DOI: 10.1111/j.1525-1594.2009.00770.x.

[24] M. Neidlin *et al.*, "A numerical framework to investigate hemodynamics during endovascular mechanical recanalization in acute stroke," no. October 2015, 2016. DOI: 10.1002/cnm.

[25] P. S. v. Schauburg *et al.*, "Mechanical and histological characterization of thrombi retrieved during thrombectomy for acute ischaemic stroke,"

[26] S. Soleimani, G. Dubini, and G. Pennati, "Possible benefits of catheters with lateral holes in coronary thrombus aspiration: A computational study for different clot viscosities and vacuum pressures," *Artificial Organs*, vol. 38, no. 10, pp. 845–855, 2014. DOI: 10.1111/aor.12274.

[27] J. Day, "Guidelines for ALE Modeling in LS-DYNA," no. July, 2009.

[28] X. J. Kaesmacher *et al.*, "Risk of thrombus fragmentation during endovascular stroke treatment," *American Journal of Neuroradiology*, vol. 38, no. 5, pp. 991–998, 2017. DOI: 10.3174/ajnr.A5105.

[29] Livermore Software Technology Corporation (LSTC), *LS-DYNA*, 0.

[30] B. Geveci, "ParaView: An End-User Tool for Large Data Visualization ParaViewWeb View project," vol. 836, 2005.

[31] G. Romero *et al.*, "A Comparison of the Removal of Blood Clots by Mechanical Thrombectomy Devices using Auto-Expandable Stents and Suction Pressure Devices," pp. 75–82, 2012. DOI: 10.5013/IJSSST.a.13.02.09.

[32] P. Inc., *MAX™ Reperfusion Catheters.*

[33] M. Mondeel, R. Cahalane, and F. Gijsen, "Review : intracranial thrombus analogs - The ultimate recipe," pp. 1–30, 2015.

[34] N. Aquelet, "ALE Adaptive Mesh Refinement in LS-DYNA," no. 2,

[35] Livermore Software Technology Corporation (LSTC), *Keyword User ' S Manual Volume 1*. 2014, vol. I, p. 2350.

[36] B. S. Freeman and J. S. Berger, "Anesthesiology Core Review Part One : BASIC Exam," in, 2014, ch. Chapter 4:

[37] K. F. Lindegaard *et al.*, "Assessment of intracranial hemodynamics in carotid artery disease by transcranial Doppler ultrasound," *Journal of Neurosurgery*, vol. 63, no. 6, pp. 890–898, 1985. DOI: 10.3171/jns.1985.63.6.0890.

[38] K.-f. Lindegaard *et al.*, "Variations in Middle Cerebral Artery Blood Flow Investigated With Noninvasive Transcranial Blood Velocity Measurements," pp. 1025–1030, 1987.

[39] R. Aaslid, T. M. Markwalder, and H. Nornes, "Noninvasive transcranial Doppler ultrasound recording of flow velocity in basal cerebral arteries," *Journal of Neurosurgery*, vol. 57, no. 6, pp. 769–774, 1982. DOI: 10.3171/jns.1982.57.6.0769.

[40] Y. Kono, "Viscosity measurement," *Magmas Under Pressure: Advances in High-Pressure Experiments on Structure and Properties of Melts*, pp. 261–280, 2018. DOI: 10.1016/B978-0-12-811301-1.00010-1.

[41] L. Antiga, B. Ene-Iordache, and A. Remuzzi, "Computational geometry for patient-specific reconstruction and meshing of blood vessels from MR and CT angiography," *Medical Imaging, IEEE Transactions on*, vol. 22, pp. 674–684, 2003. DOI: 10.1109/TMI.2003.812261.

[42] O. K. Baskurt, *Handbook of hemorheology and hemodynamics*. 2007, vol. 69, pp. 1–455.

[43] C. Mechanics, *Methods in Cell Biology*.

[44] M. I. Worldwide, "WHITEPAPER A Basic Introduction to Rheology," 2016.

[45] C. Mrazek *et al.*, "The relationship between vacuum and hemolysis during catheter blood collection: A retrospective analysis of six large cohorts," *Clinical Chemistry and Laboratory Medicine*, vol. 55, no. 8, pp. 1129–1134, 2017. DOI: 10.1515/cclm-2016-0940.

[46] F. Lally *et al.*, "In vitro experiments of cerebral blood fl ow during aspiration thrombectomy : potential effects on cerebral perfusion pressure and collateral fl ow," pp. 969–972, 2016. DOI: 10.1136/neurintsurg-2015-011909.